Chapter 3

A Methodology to Interpret Climate Change Due to Influences of the Orbital Parameter on Changes of Earth's Rotation Rate and Obliquity

Xinhua Liu

Additional information is available at the end of the chapter

http://dx.doi.org/10.5772/54811

1. Introduction

Astroclimatology is the branch of paleoclimatology in which climate change over geological history is interpreted in terms of changes in astronomical elements or in the Earth's orbital parameters. There are two mature theories in astroclimatology. Milankovitch theory considers the Pleistocene glacial cycles to be the result of tiny changes in three orbital elements (obliquity, eccentricity, and the equation of the equinoxes) (Berger, A., *et al.*, 1984). Another theory proposes that oscillations between glacial and interglacial periods result from large fluctuations of obliquity (Williams, G. E., 1981). It is clear that changes in orbital parameters can have an important effect on climate. Reconstructions of paleoclimate and its simulation are vital for us to understand the evolution of climate and to forecast future climate change.

The influences of the orbital parameters have multiple time scales from several hours to geological time scales. Zheng (1994) and Qian *et al*. (1995) investigated the influence on the atmosphere and ocean of changes in the Earth's rotation rate on a time scale of less than 100 years, using observations combined with a dynamic method. The results suggest that the rotation rate of the Earth has a close relationship with Southern Oscillation, El Nino, magnitude and location of the Subtropical High, sea surface temperature, and precipitation, respectively. These researches have deepened our knowledge of the relationship between rotation rate and the atmosphere and ocean. Long-term changes in rotation rate and changes in other orbital parameters can also affect the atmospheric circulation and have generally been investigated through numerical simulations of paleoclimate. The aim of paleoclimate research is to use our knowledge of paleoclimate change to understand the mechanism of climate change, and thus to improve our ability to forecast climate change. Models used in the simulation of paleoclimate include Box Models, Energy Balance Models (EBMs),

Statistical-dynamical Models (SDMs), Radiative Convective Models (RCMs), Earth System Models of Intermediate Complexity (EMICs) and General Circulation Models (GCMs). This study focuses on GCMs.

1.1. Review on the simulation of influence of orbital parameter change in specific geological period on atmosphere

1.1.1. Numerical simulation of paleoclimate

Numerical simulations are important in paleoclimatological research. The earliest numerical simulations of paleoclimate were carried out in the 1970s (Williams *et al*., 1974). Since then the simulation time scale has been extended from short-time-scale rapid climate change and orbital-time-scale climate change to climate change at the geological time scale (Kutzbach and Street-Perrott, 1985; Kutzbach, 1989; Rahmstorf, 1994). Simulations have been carried out for the Holocene, Pleistocene, Pliocene, early Cenozoic, and Cretaceous geological periods, extending to the time of the Pangaea supercontinent (Kutzbach and Gallimore, 1989; Barron *et al*., 1993; Barron *et al*., 1995; Kutzbach, 1996; Bush and Philander, 1997; Otto-Bliesner and Upchurch Jr, 1997; Ramstein *et al*., 1997; Cane and Molnar, 2001). Different climate driving factors have been investigated, including changes in orbital parameters, CO_2 concentration and global ice quantity, and thermohaline circulation changes resulting from closed and open ocean channels, plateau uplift, and plate tectonics (Kutzbach and Guetter, 1986; Mitchell *et al*., 1988; Kutzbach and Gallimore, 1989; Barron *et al*., 1993; Kutzbach *et al*., 1993; Barron *et al*., 1995; Rahmstorf, 1995; Ramstein *et al*., 1997; Weaver *et al*., 1998; Cane and Molnar, 2001; Knutti *et al*., 2004).

1.1.2. Simulation of glacial cycle

The international research effort on glacial cycle simulation has taken the form of a series of large projects, including CLIMAP (Climate Long-range Investigation, Mapping, and Prediction), COHMAP (Cooperative Holocene Mapping Project), and PMIP (Paleoclimate Modeling Intercomparison Project).

CLIMAP is a reconstruction of the earth's environment during the ice age. Carried out in the 1970s, it was led by the marine geologists J. Imbrie and J. Hays, and the geochemist N. Shackleton. Using data related to the reconstructed environment of the ice age, the CLIMAP project simulated the summer climate at the Last Glacial Maximum (LGM). The results show that the global summer climate was drier and colder during the LGM than at present. At the same time, the westerlies over the Northern Hemisphere near the ice cap move southward obviously (Gates, 1976).

In the 1980s, COHMAP, led by J. E. Kutzbach, T. Webb III, and H. E. Wright, was designed to determine and simulate paleoclimate using the land record. It revealed the key role of orbital factors in tropical monsoon climate change, and the bifurcation of the westerly jet stream over North America as a result of the ice cap in North America during the LGM period. Simulations showed that the change of Earth's orbit in the early to middle Holocene

led to an increase in seasonality in the Northern Hemisphere and an enhanced monsoon (Kutzbach and Street-Perrott, 1985; Kutzbach and Guetter, 1986; Mitchell *et al*., 1988; Kutzbach, 1989; Kutzbach and Gallimore, 1989; Barron *et al*., 1993; Kutzbach *et al*., 1993; Rahmstorf, 1994; Barron *et al*., 1995; Rahmstorf, 1995; Kutzbach *et al*., 1996; Bush and Philander, 1997; Otto-Bliesner and Upchurch Jr, 1997; Ramstein *et al*., 1997; Weaver *et al*., 1998; Cane and Molnar, 2001; Knutti *et al*., 2004). This coincided with generally high lake levels during 9–6 Ka BP (Kutzbach, 1985).

The PMIP, part of Past Global Changes Project (PAGES), in the 1990s was led by S. Joussaume, with contributions from a number of leading paleoclimate scientists including J. E. Kutzbach, A. J. Broccoli, and J. Guiot *et al.*. This research project evaluated the sensitivity and accuracy of models by comparing results from different climate models and the difference between the simulation results and observational record. In general, the models all simulated the main features of climate change since the LGM, including the monsoon enhancement driven by orbital factors in the early to middle Holocene (6 Ka BP) and the enhanced meridional temperature gradient during the LGM period (Joussaume and Taylor, 1995). The simulations significantly underestimated the range of climate change evident in the record. The tropical Atlantic Ocean warming further enhanced the African monsoon in the middle Holocene (Kutzbach *et al*., 1996; Kutzbach and Liu, 1997).

1.1.3. Simulation before the Pleistocene

Because it is difficult to reconstruct the boundary conditions of the Pleistocene, simulations of the climate before the Pleistocene differ from simulations of glacial cycles in the Quaternary, in that their focus is not on reconstruction, but on sensitivity testing. Prell and Kutzbach (1997) investigated the response of the monsoon to orbital change and its association with the Qinghai–Tibet Plateau height and uplift mode. The results showed a remarkable orbit-driven effect of the uplift mode on monsoon response. Under the mode of stable plateau uplift in the past 15 Ma, monsoon intensity and variable rate index have shown little change, whereas under the mode of large uplift at 11–8 Ma, monsoon intensity and the variable rate index showed a marked increase. These results show that the sensitivity of the orbit-driven monsoon response has strengthened greatly. Under the Quaternary uplift mode, monsoon intensity and variability increased abruptly at 2–3 Ma. This shows that not just the rate of plateau uplift, but also the process and mode of uplift may have an important influence on climate change.

1.2. Review on the simulation of influence of orbital parameter change in non-specific geological period on the atmosphere

Hunt (1979) investigated the effects of a five-fold increase or decrease in rotation rate. The lower rotation rate resulted in phenomena including enhanced mid-latitude westerly jet stream, a decrease in the tropospheric temperature gradient with warming in polar regions, and an expansion of the subtropical arid area. The rapid rotation scenario yielded a

significant tropospheric zonal temperature gradient and dry, cold high latitudes. A hemispheric model was used without terrain changes or diurnal processes, considering yearly average cloud, ozone, and ground reflectivity. Because the terrain and the land–sea distribution are different between the Northern and Southern Hemisphere, the anomalies of the atmospheric circulation and climate caused by change in Coriolis force are not hemispherically symmetrical. Therefore, the changes of circulation and climate in the two hemispheres and the differences between the two hemispheres are not depicted well in the model. Furthermore, the monthly and seasonal differences of all sorts of effects cannot be considered in this model.

Kutzbach and Otto-Bliesner (1982) analyzed the effect of orbital parameter change in the Holocene on the African and Asian monsoon. The difference of radiation is largest at the two solstitial points, and two solstitial points are closely related to the monsoon; therefore, the effects of different orbital parameters on the monsoon in summer and winter were analyzed. The results showed that the monsoon in the Holocene was stronger than now and that precipitation in Africa and India was heavier. The seasonal circulation corresponding to different orbital parameters was not discussed in detail.

Even though Kutzbach and Guetter (1986) discussed the effect of different orbital parameters and surface boundary conditions on the climate, the radiation and sea temperature conditions were fixed to January and July conditions. Again, there was no detailed discussion of the effect of different orbital parameters on climate under seasonal cycle. Their conclusion was that the response of the monsoon and tropical precipitation to the change of radiation caused by change in orbital parameter is stronger than the response of the forcing. Similar conclusions were made to those in Kutzbach and Otto-Bliesner (1982).

Using the NCAR Community Climate Model version 0 (CCM0), Jenkins (1993) investigated the effect of a high rotation rate on circulation. Terrain was not considered. The radiative forcing was reduced by 10% from present values, as an approximation of the radiation incident on the early Earth. The carbon dioxide concentration in the atmosphere was higher than present values, and other forcings were annual averages. It was concluded that by reducing the cloud amount, a high rotation rate influences the climate. Using the same model, Jenkins *et al.* (1993) investigated the effect of the presence or absence of land and of rapid rotation rate on the climate at 2.5–4 billion years ago, yielding the following results:

1. When the day length is 14 hours, the world average cloud coverage drops to 79% of the present value and the global average temperature rises by 2 K.
2. In the absence of land, the global average temperature rises by 4 K compared with the present value.
3. Increasing the rotation rate and reducing the land area offsets the impact of lower solar radiation during early times on the Earth. Therefore the early Earth might not have needed more CO_2 to maintain its temperature above freezing point.
4. The surface wind direction reversed from west to east in mid-latitudes with the high rotation rate of the early Precambrian, and the meridional mean surface wind was

enhanced. Compared with the current single jet stream, it is possible that there were two jet streams in the early Earth.

Jenkins (1996) then used the NCAR CCM1 model to investigate the effect of a high rotation rate on the climate, using the present-day land–sea distribution, CO_2 concentration, and ozone concentration. The climatological January mean sea surface temperature field and radiative forcing were used in the model, yielding the following conclusions:

1. Polar temperatures fall under the high rotation rate and the winter hemisphere is noticeably colder. As rotation rate increases, the permanent ridge and trough features weaken. When the length of day is less than 18 hours, the ridge and trough features disappear completely.
2. Under fast rotation there is strong mid-latitude subsidence, which is more pronounced in the Pacific and Atlantic.
3. While present-day storm trajectories are mainly controlled by large-scale fluctuation, the trajectories under fast rotation consist of small-scale fluctuations. This kind of movement forward to the small-scale fluctuation under the high rotation rate is related to enhanced convective precipitation.

Hall *et al*. (2005) investigated the effect of a change in orbital parameter on the climate in winter in the Northern Hemisphere using an atmosphere–ocean coupled model employing orbital forcings for the past 165,000 years. The results suggest that while global summer temperature differences can be explained by local thermodynamics caused by a change in radiative forcing, the change of winter climate in the Northern Hemisphere cannot be explained completely in this way. The authors concluded that the change in radiative forcing gave rise to an atmospheric circulation anomaly similar to the Northern Hemisphere Annular Mode (NAM). This circulation anomaly perturbed other climatological variables.

1.3. Discussion and future prospective

Research on the effect of orbital parameter change on circulation and climate has deepened our understanding of the paleoclimate, but previous simulations focused on a specific geological period or specific seasons (mostly summer and winter). The influence of a single orbital parameter change on the circulation has never been examined in detail. Moreover, analyses of sediment in the Arabian and South China seas show that variations in global ice-cover have an important influence on the east Asian monsoon, while orbital parameters, especially the change of precession, are the main external driving force for the east Asian summer monsoon and Indian summer monsoon (Clemens *et al*., 1991; Jian *et al*., 2001). Previous studies considered the effect of orbital parameters on the monsoon within a limited area, but the effect of orbital parameters on the global monsoon has rarely been considered. Liu *et al*. (2010) and Liu (2011) therefore investigated the effect of rotation rate and obliquity on global circulation, describing the responses of atmospheric elements and three-cell circulation to variations in a single orbital parameter. Furthermore, they discussed the response of the global monsoon to different rotation rates. Their conclusions are that the African monsoon and the monsoon in the temperate and frigid zones weaken when the

rotation rate slows, and vice versa, while the Asia–Australia monsoon has no obvious reverse change with a change of rotation rate. The monsoon changes are different with rotation rate in different areas. However, these studies are somewhat preliminary in nature, and future research on the effect of different orbital parameters on circulation could include the following aspects:

1. Consideration of changes in each of the three key elements of the Earth's orbit, using a GCM to simulate the circulation. This will identify the relative effects of the three orbital elements.
2. An atmosphere–ocean coupled model could be used to investigate the effects of different orbital parameters on the circulation. The mechanisms by which the ocean and atmosphere influence each other under the change of orbital parameter should be discussed in more detail in the future.

2. The influence of different rotation rates on the general circulation of the Earth's atmosphere

The observations of celestial optics and modern spatial geodesy have proved that the rotation of the Earth varies on multiple time scales ranging from several hours to geological ages, and fossil analysis has shown that the Earth's rotation rate is currently slowing. Changes in the Earth's rotation can have an important effect on the atmosphere.

Numerical simulations of the influence of change in rotation rate on geological time scales on the atmospheric circulation and climate have greatly improved our understanding of the ancient climate (Hunt, 1979; Kutzbach and Otto-Bliesner, 1982; Kutzbach and Guetter, 1986; Jenkins, 1993, 1996; Jenkins *et al.*, 1993; Hall *et al.*, 2005). However, this research has either focused on a specific geological period or on specific seasons (mostly summer and winter). The influence of a single orbital parameter change on the circulation has not been studied. Moreover, Jenkins (1996) reported a threshold at a day length of 18 hours: when the day length is shorter than 18 hours, the atmospheric circulation will change significantly. The same conclusion can be drawn from numerical simulations in which the meridional circulation changes from two circuits to a single circuit, when the day length increases from 16 to 64 times its present-day length (Del Genio, 1996). What happens when the day length changes by one hour? Is the atmospheric change significant? Based on the above considerations, the present study performed simulations to investigate the atmospheric circulation under different rotation rates.

2.1. Model description and experimental design

The atmospheric general circulation model (AGCM) used in this study is the NCAR Community Atmospheric Model version 2 (CAM2) released in July 2003. CAM2 uses spherical harmonic functions truncated at wave number 42. To facilitate physical computing, the model grids are based on 64 latitude Gaussian points and 128 longitude points (2.8125 degree intervals) in the horizontal plane, with 26 hybrid vertical levels. The

model includes detailed radiative forcing, cumulus convection, and a land surface process parameterization scheme. The sea surface temperature (SST) adopted is the climatological average SST field. Present-day terrain is used. A complete description of this model version is available online at http://www.ccsm.ucar.edu/models/atmcam/docs/description/index.html. A control run with 24-hour day length and two sensitivity runs, with 23- and 25-hour day length, are discussed in this section. These two sensitivity runs represent a condition from geological history and some 10,000 years in the future, respectively. The time series of whole layer average dimensionless angular momentum and the integrals of unit quality atmospheric kinetic energy in the troposphere (surface–100 hPa) and stratosphere (100 hPa–stratosphere top) in the sensitivity runs show that the atmospheric conditions reach steady state after two years (figure not shown). The whole-layer averaged dimensionless angular momentum is an index of atmospheric rotation, which is defined as the ratio of the specific angular momentum $a\cos\phi(u + a\Omega\cos\phi)$ to the mean specific angular momentum of the atmosphere at rest $2a^2\Omega/3$ (Hourdin *et al*., 1995). We run a 32-year simulation. The first two years are considered as spin-up, and only the results of the last 30 years are analyzed.

2.2. The results of climatic annual mean atmospheric circulation under different rotation rates

The wind speed difference can be used as a representation of the strength of the three-cell circulation (Oort and Yienger, 1996; Quan *et al*., 2004). With increasing day length, the strength changes of the three-cell circulation are different for the two hemispheres and at different latitudes, while the extent of the three-cell circulation does not change significantly. Figure 1 shows that the change under the higher rotation rate is opposite to

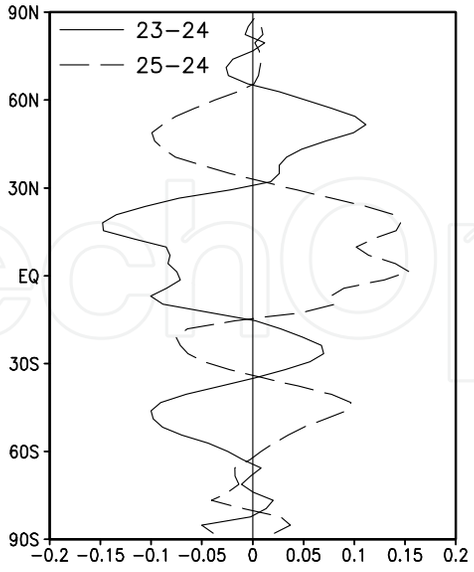

Figure 1. Three-cell circulation index (high-level meridional wind minus low-level meridional wind) obtained by subtracting the control run from the sensitivity run for the climate annual mean. The solid line is the 23-hour day sensitivity run minus the control run. The dashed line is the 25-hour day sensitivity run minus the control run. Units: m s^{-1}.

that under the lower rate. The three-cell circulation is stronger with slower rotation than with faster rotation. It should be pointed out that the changes of circulation at latitudes south of 80°S and between 10°S–10°N do not behave in this way. In these regions the circulation strength decreases under the slow rotation, and increases under faster rotation compared with the control run. In general, the main characteristics are that the circulation strength increases globally when the rotation slows, and vice versa.

Results for the temperature field are as follows (Fig. 2). There are cold anomalies in the Northern Hemisphere and warm anomalies in the Southern Hemisphere for the lower rotation rate, while the opposite applies for the higher rate. The boundary between cold and warm anomalies is at 15°S. The trend of geopotential height change is the same as for the temperature field between different rotation rates (figure not shown).

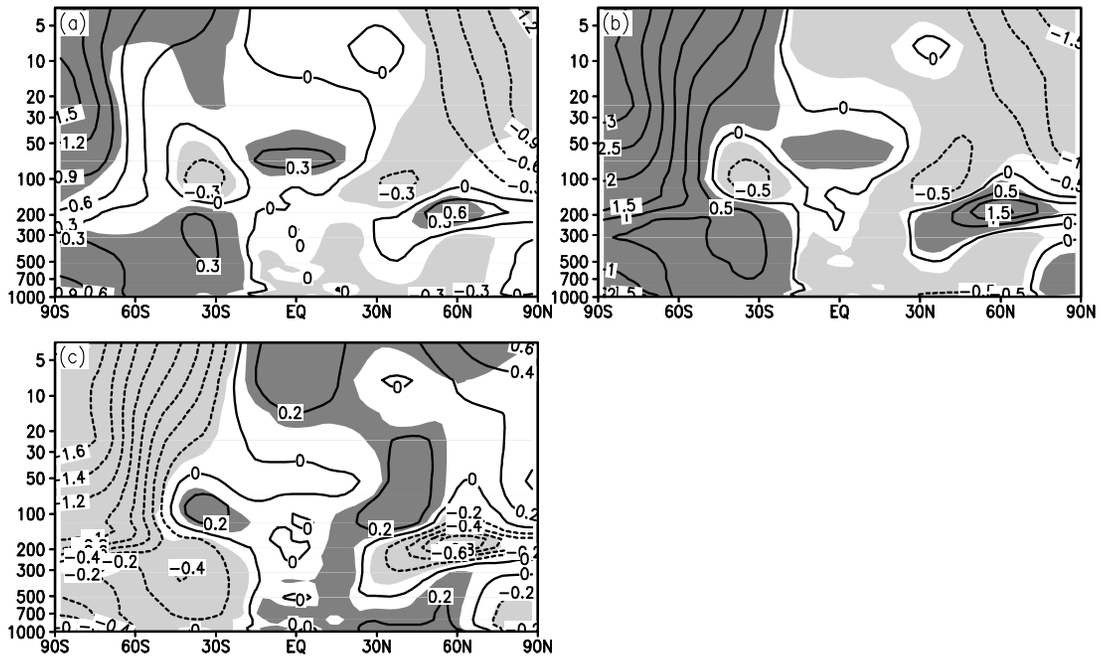

Figure 2. Latitude–pressure cross-section of climatological annual temperature anomaly field, which is the sensitivity run minus the control run. a) 25-hour day minus 24-hour day; b) Same as a) but for 25-hour minus 23-hour; c) Same as a) but for 23-hour minus 24-hour. The shaded areas indicate significant difference at the 95% level according to Student's *t*-test. Positive anomalies are shown by dark shading, negative ones by light shading. Units: K.

The sign of the annual mean zonal wind field anomalies changes when the rotation rate is changed (Fig. 3). The positive and negative anomalies reverse between higher and lower rotation rates. Westerlies are strengthened in the middle-higher latitudes (40°S–60°S and 40°N–60°N) under the lower rotation rate, and weakened elsewhere. The reverse situation applies under the higher rotation rate, but at slightly different latitudes. Compared with the control run, with slow rotation the easterlies strengthen and westerlies weaken at 15°S–30°S and below 700 hPa over the region 0°–30°N. Westerlies strengthen and easterlies weaken above 500 hPa at 30°S–70°S and 15°S–60°N. The situation reverses under the higher rotation rate. As the rotation rate becomes even slower, the extent of the positive and negative areas

also increase. Convergence and divergence of the tropospheric wind field are enhanced when the rotation rate decreases (figure not shown). Vertical velocities are enhanced in the troposphere and north of 30°S in the stratosphere with a lower rotation rate, while the vertical velocity weakens south of 30°S in the stratosphere. The situation with a higher rotation rate reverses, but the change is not completely symmetrical (figure not shown).

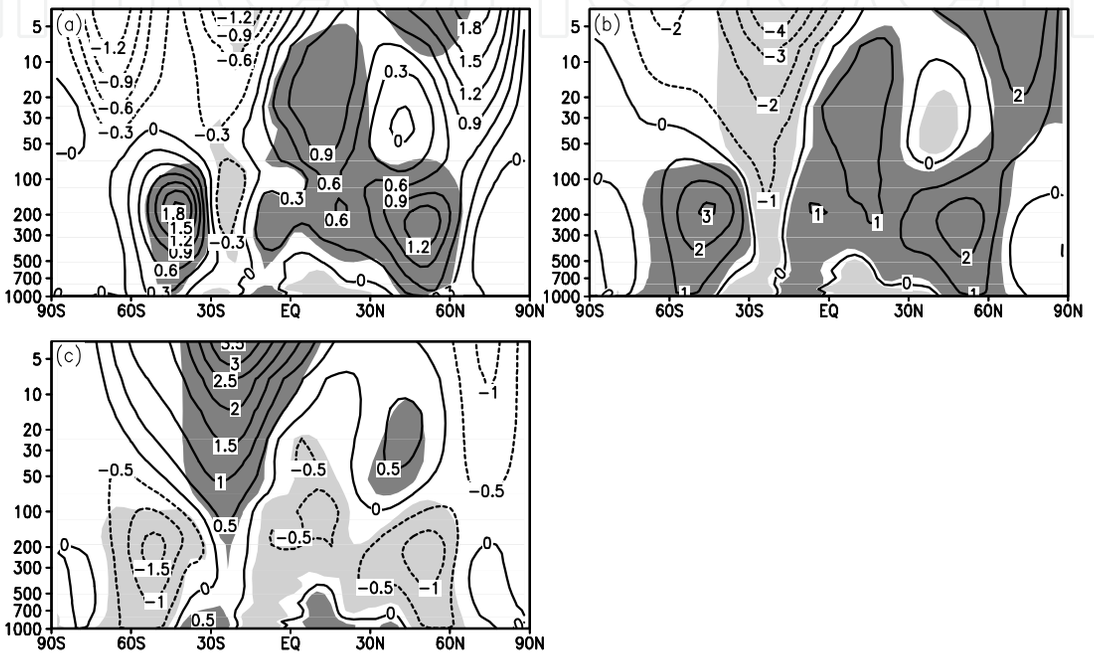

Figure 3. Same as Fig. 2 but for zonal wind. Units: m s^{-1}.

2.3. The results of climatic seasonal mean atmospheric circulation under different rotation rates

Figure 4 shows the changes in the climatological seasonal mean three-cell circulations with different rotation rates. The changes of three-cell circulation in the Northern and Southern Hemispheres are not consistent under different rotation rates. In the Northern Hemisphere the three-cell circulation strengthens under the slower rotation and weakens under the faster rotation. Enhancement of the three-cell circulation is not obvious in the Southern Hemisphere. Autumn changes in the ascending branches of the Hadley cell over the low-latitude (0°–25°S) Southern Hemisphere and in the Ferrel cell over high latitudes (60°S–90°S) are not consistent with changes in other seasons, which show weakening under the lower rotation rate and strengthening under the higher rate. The changes in strength of the three-cell circulation in autumn are the most obvious. For the Hadley cell, the change in strength in winter is the second most obvious. The changes in the climatological annual mean three-

cell circulation are affected by those of the climatological seasonal mean three-cell circulation.

The magnitudes of change vary significantly with season, with the change in autumn being the largest. The largest changes in strength and extent of geopotential height under different rotation rates are seen in the autumn. The changes in spring under different rotation rates of geopotential height field, temperature field, meridional wind field in the stratosphere and vertical velocity field are opposite to those in summer and winter (and to the annual mean). Westerlies in mid-latitudes are strengthened in all four seasons with slow rotation. Changes in the zonal wind in the two hemispheres are opposite in spring and autumn.

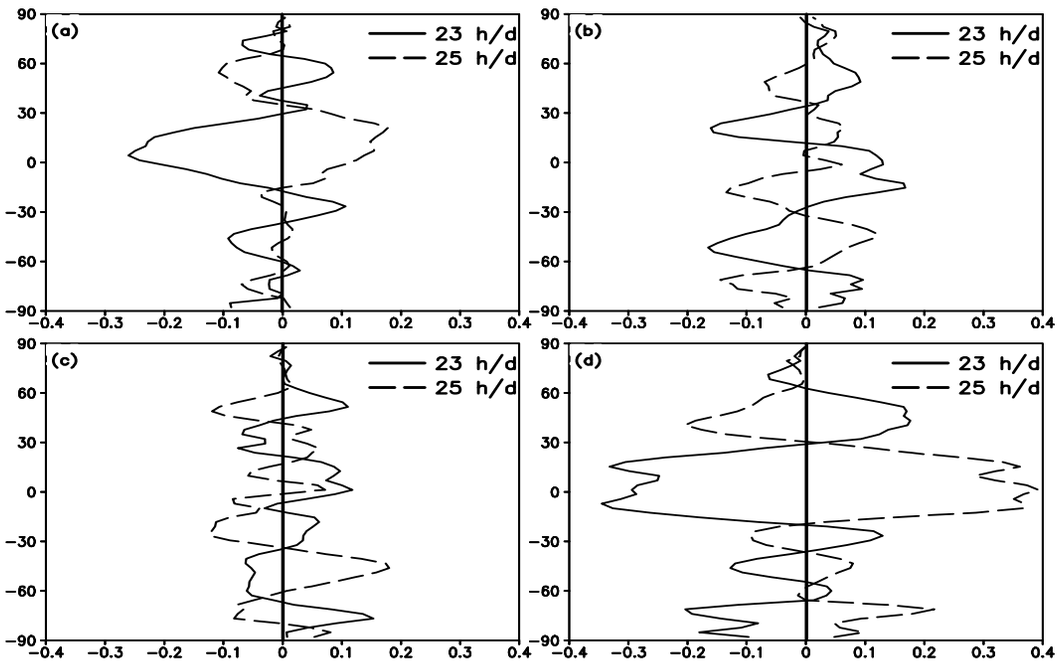

Figure 4. Same as Fig. 1 but for seasonal mean. The solid line and the dashed line are 23 h/d and 25 h/d, respectively. a)–d) are the situations in winter, spring, summer, and autumn, respectively. Units: m s^{-1}.

2.4. Concluding remarks

The general circulation of the Earth's atmosphere has been modeled under different rotation rates using the NCAR CAM2 model. The results indicate that the intensity of the three-cell circulation strengthens when the rotation rate slows. Slower rotation gives cold anomalies in the annual mean temperature field in the Northern Hemisphere and warm anomalies in the Southern Hemisphere, with the boundary between cold and warm anomalies located at 15°S. The annual mean zonal wind field has positive and negative anomalies when the

rotation rate is changed. The positive and negative anomalies reverse between higher and lower rotation rates. In spring, the changes of geopotential height field, temperature field, meridional wind field in the stratosphere, and vertical velocity field are opposite to those in summer and winter (and the annual mean) under different rotation rates. Westerlies in mid-latitudes strengthen in all four seasons with slow rotation. Trends in the zonal wind changes in the two hemispheres are opposite in spring and autumn. Quantitative changes have significant seasonal differences, with the largest changes in autumn.

3. The influence of different obliquity on the general circulation of the Earth's atmosphere

The obliquity of the Earth ranges from 21.6° to 24.5° over a 41,000-year cycle. The obliquities of other planets and dwarf planets with atmospheres in our solar system range from 3° to 120°. Each atmosphere has its own characteristics. How does a change in obliquity influence atmospheric circulation?

Determining the influence of obliquity change over geological time scales involves the reconstruction and numerical simulation of paleoclimate. Kutzbach and Otto-Bliesner (1982) analyzed the effect of orbital parameter change in the Holocene on the African and Asian monsoons. The effects of different orbital parameters on the monsoon in summer and winter were analyzed in detail, revealing that the monsoon in the Holocene was stronger than now and that precipitation in Africa and India was heavier than now. The effect on seasonal global circulation of changes in the orbital parameter was not discussed in detail. Although Kutzbach and Guetter (1986) discussed the effect of different orbital parameter and surface forcing conditions on the climate, the radiation and sea temperature conditions were fixed at January and July values. The authors provided no detailed discussion of the effect of different orbital parameters on the seasonal cycle. Hall *et al*. (2005) investigated the effect of change in orbital parameter on the climate in winter in the Northern Hemisphere using an atmosphere–ocean coupled model with orbital parameters from the past 165,000 years. Their results suggest that while differences in global summer temperature can be explained by local thermodynamics caused by changes in radiative forcing, the change of winter climate in Northern Hemisphere cannot be explained in this way. They proposed that the change of radiative forcing has generated an atmospheric circulation anomaly similar to the NAM. This circulation anomaly perturbed other climatological variables. Tuenter *et al*. (2003) investigated the effects of procession and obliquity on the African monsoon. Past research on the effect of orbital parameter changes over geological scales on circulation and climate has deepened our understanding of paleoclimate, but these simulations have either focused on a specific geological period or a specific season (mostly summer and winter). The influence of a single orbital parameter change on the circulation has never been examined in detail. Moreover, there has been little work on the effect on the seasonal general circulation. The influence of different rotation rates on the atmospheric circulation was studied in the last section; in this section, we consider the influence of obliquity on the general circulation.

3.1. Model description and experimental design

In this section we use the same model as in Section 2. In addition to the control run, sensitivity runs with obliquities of 0°, 20°, 30°, and 60° are discussed. The same methods are used to judge whether the model is stable. We run a 32-year simulation; again, only the last 30 years are analyzed.

3.2. The results of climatic annual mean atmospheric circulation under different obliquities

Figure 5 shows that the intensity of the three-cell circulation weakens with increasing obliquity. The ascending branch of the Hadley cell in the Southern Hemisphere is enhanced with an obliquity of 60°. With obliquity increased, the Hadley cell in the Southern Hemisphere expands, and the Hadley cell in the Northern Hemisphere and the Ferrel cell in the Southern Hemisphere contract. It should be noted that the three-cell circulation in the Southern and Northern Hemispheres is not symmetric at an obliquity of 0°, possibly because of the asymmetry between the terrain in the Southern and Northern Hemispheres, or because the temperature forcing used in the model is the annual climatological mean. This latter factor can also cause the asymmetry of the three-cell circulation between the Northern and Southern Hemispheres at an obliquity of 0°. Compared with the control run, the distributions of anomalies are very similar for the sensitivity runs of 0° and 60°, and those of 20° and 30°, while the anomaly magnitudes of 0° and 60° are larger than those of 20° and 30°. There is a linear weakening in the three-cell circulation with increasing obliquity.

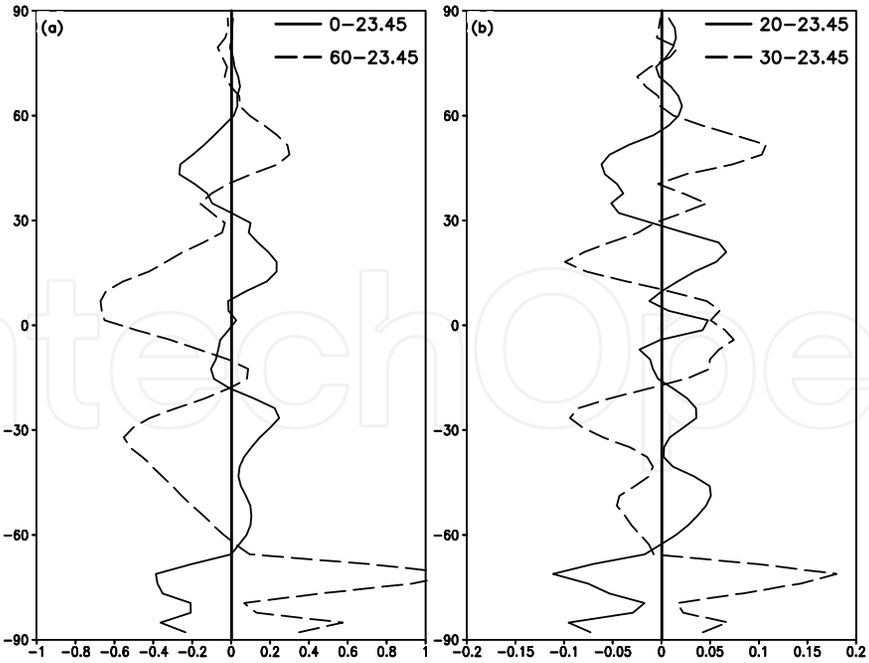

Figure 5. Three-cell circulation index (high-level meridional wind minus low-level meridional wind) for different obliquities, obtained by subtracting the climate annual mean control run from the sensitivity run. a) Solid line represents 0° minus 23.45°. The dashed line represents 60° minus 23.45°; b) Same as a) but for 20° minus 23.45° (solid line) and 30° minus 23.45° (dashed line). Units: m s^{-1}.

These variations in the three-cell circulation can be explained as follows. As obliquity changes, the highest latitude that sunlight can reach at winter solstice and summer solstice will change. The larger the obliquity, the higher the latitude that sunlight can reach. The radiation received throughout the year at high latitudes increases, while that received at low latitude decreases. This pattern necessarily weakens ascent over the equator and descent over the polar regions, so that the Hadley and anti-Hadley cells are weakened. Furthermore, the Ferrel cell is weakened.

Latitude–pressure cross-sections of the climate-mean annual geopotential height anomaly (figure not shown), which is the sensitivity run minus the control run, show that the positive anomaly mainly lies at 30°S–30°N (reaching a maximum of 205 gpm and 60 gpm, respectively) with smaller obliquity. The negative anomaly lies south of 30°S and north of 30°N, and the anomaly in the Northern Hemisphere is larger than that in the Southern Hemisphere. The situation reverses when obliquity is increased. There are increases in geopotential height at 30°S–30°N, and decreases south of 30°S and north of 30°N, with the obliquity decreased. The change of geopotential height with the obliquity change is larger in the Northern Hemisphere than in the Southern Hemisphere.

Figure 6 shows latitude–pressure cross-sections of the climate-mean annual temperature anomaly field. Consistent with the changes in geopotential height field, a reduction in obliquity to 0° and 20° gives positive anomalies at 30°S–30°N (reaching a maximum of 4 K and 1.2 K, respectively), with negative anomalies south of 30°S and north of 30°N. The situation reverses under larger obliquity. At an obliquity of 0°, there is a zone of positive temperature anomaly at 10 hPa over the South Pole region, extending northward and downward, reaching 45°S near the surface. At an obliquity of 60°, there is a region of positive anomaly between 100 to 200 hPa over the equator.

Latitude–pressure cross-sections of climate-mean annual zonal wind anomaly field (not shown) show that the extent of easterlies in the stratosphere over the equator with an obliquity of 0° is smaller than that in the control run, while with an obliquity of 20°, it is close to that in the control run. The extent of easterlies in the stratosphere over the equator with an obliquity of 30° is slightly larger than in the control run and is largest in these simulations for an obliquity of 60°. The velocity of the easterlies in the stratosphere over the equator increases with increasing obliquity. Easterly velocities can reach 80 m s^{-1} when the obliquity is 60°. The extent of the westerlies decreases with increasing obliquity. At the same time the extent of the jet stream is reduced. The jet stream at middle latitudes in the Northern Hemisphere decreases from 30 to 10 m s^{-1} when the obliquity increases from 0° to 60°. The strongest winds at high latitudes in the Northern and Southern Hemispheres decrease from 20 to 10 m s^{-1} and from 50 to 40 m s^{-1}, respectively.

Figure 7 shows the situation with obliquity reduced from 23.45° (Fig. 7a and b). The easterlies strengthen and westerlies weaken below 500 hPa over 30°S–45°S and 10°S–20°S, and below 300 hPa over 10°N–20°N and 60°N–90°N. At the same time, easterlies weaken and westerlies strengthen in the troposphere over 45°S–80°S, 20°S–30°S, 10°S–10°N, and 35°N–60°N. Easterlies weaken and westerlies strengthen south of 45°S in the stratosphere

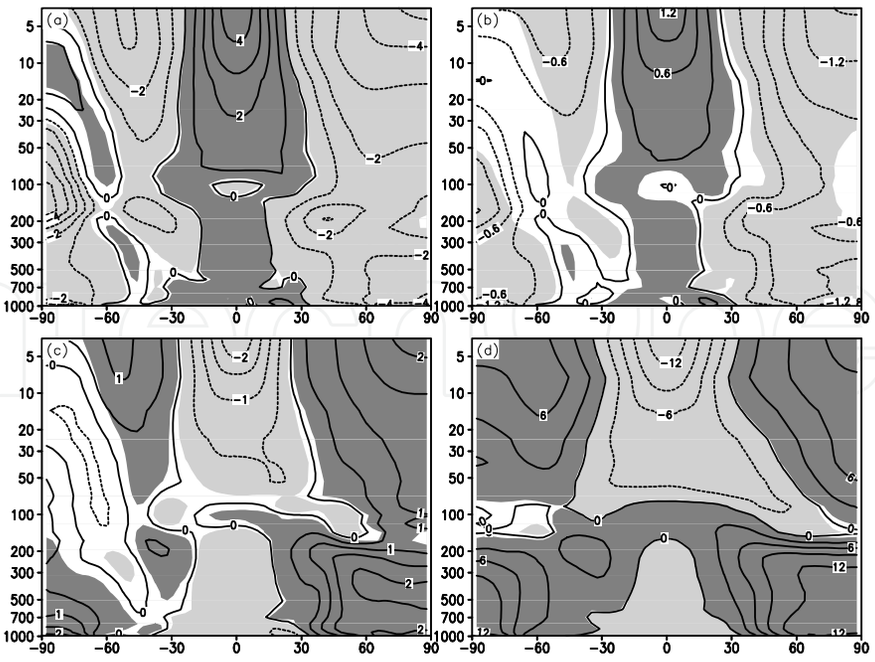

Figure 6. Latitude–pressure cross-section of climate-mean annual temperature anomaly field, which is the sensitivity run minus the control run. a) 0° minus 23.45°; b) 20° minus 23.45°; c) 30° minus 23.45°; d) 60° minus 23.45°. Units: K. The shaded areas are significant at the 95% level according to Student's *t*-test. Dark shading indicates positive anomaly, light shading indicates negative anomaly.

and over 40°S–60°N. With obliquity greater than 23.45° (Fig. 7c and d), easterlies weaken and westerlies strengthen over 80°S–90°S below 500 hPa, 30°S–45°S, 10°S–20°S below 300 hPa, 10°N–20°N below 300 hPa, and over 60°N–90°N. The easterlies strengthen and westerlies weaken over 45°S–80°S in the troposphere, and over 20°S–30°S, 10°S–10°N, and 35°N–60°N. The easterlies strengthen and westerlies weaken south of 45°S in the stratosphere and over 40°S–60°N.

To summarize, the effect of increased obliquity is as follows. The extent of easterlies in the stratosphere increases and wind velocity strengthens. The extent of westerlies in the Southern and Northern Hemispheres is reduced. The jet stream in the Northern Hemisphere weakens, while that in the Southern Hemisphere strengthens. Except for the strengthening of easterlies over 10°S–10°N, the wind fields over other regions near the surface weaken. The pattern with reduced obliquity is reversed.

For the annual-mean meridional wind field (not shown), as obliquity is increased the strengths of the three-cell circulation, convergence, and divergence all weaken. With increasing obliquity, southerlies weaken and northerlies strengthen south of 50°S in the stratosphere and north of 40°N. Northerlies weaken over 50°S–0° below 5 hPa in the stratosphere, while southerlies weaken over 0°–25°N. Northerlies above 5 hPa over 50°S–0° and southerlies above 5 hPa over 0°–25°N strengthen.

For the vertical wind field (figure not shown), the results in the troposphere are consistent with the change of three-cell circulation and meridional wind field. With increasing obliquity the vertical wind velocity decreases. In the stratosphere, the ascent strengthens

over 45°S–65°S, 25°S–25°N, and 60°N–90°N, and weakens over 65°S–90°S. Descent strengthens over 25°S–45°S and 25°N–45°N.

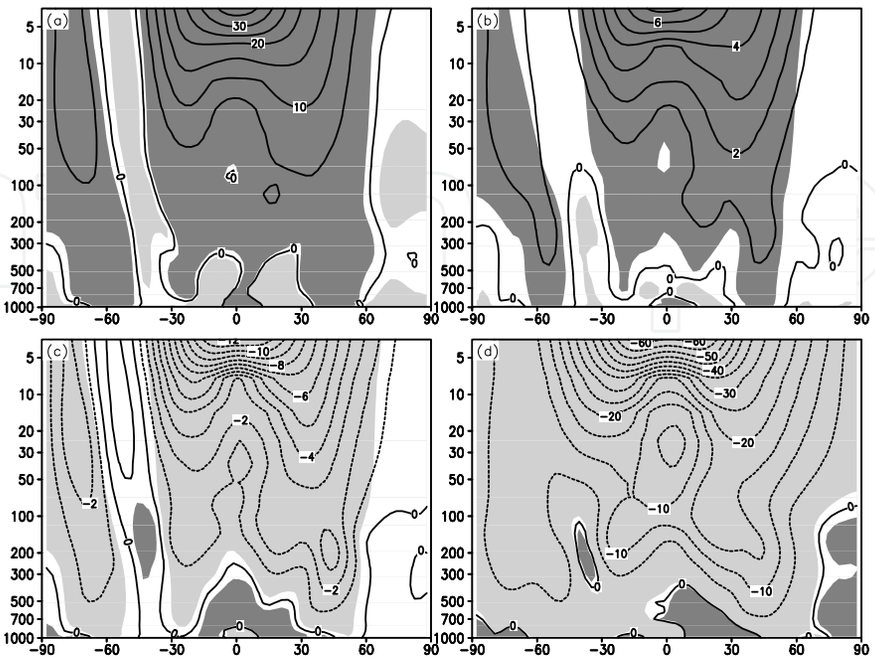

Figure 7. Same as Fig. 6 but for zonal wind field. Units are m s^{-1}.

3.3. The results of climatic seasonal mean atmospheric circulation under different obliquities

For the three-cell circulation, the results of increased obliquity are as follows (Fig. 8). The three-cell circulation in the Northern Hemisphere strengthens in winter, and that in the Southern Hemisphere weakens. The three-cell circulation in the Northern Hemisphere weakens in spring, and the Hadley cell in the Southern Hemisphere strengthens. The other two cells weaken in the Southern Hemisphere in spring. In summer, the three-cell circulation weakens in the Northern Hemisphere, and the Hadley cell in the Southern Hemisphere strengthens. At the same time, the changes of the other two cells are not obvious. In autumn, the global three-cell circulation weakens. The trend of changes in the three-cell circulation in the Northern Hemisphere in winter, and the Hadley cell in the Southern Hemisphere in spring and summer are opposite to the corresponding trends of the annual mean. The changes in strength of the three-cell circulation in winter and summer are larger than in the other two seasons. With the exception of the Northern Hemisphere three-cell circulation in winter and the Southern Hemisphere Hadley cell in spring and summer, which strengthen with increased obliquity, the general trend is for cells to weaken.

The results for the geopotential height field with increased obliquity are as follows (figure not shown). In spring the geopotential height decreases over 60°S–20°N, and increases south of 60°S and north of 20°N. In summer the geopotential height increases north of 30°N and over 40°S–30°N at 100–20 hPa, while it decreases below 100 hPa over 30°S–30°N, above 5 hPa at 30°S–30°N, and south of 30°S. In autumn the geopotential height decreases over 30°S–

30°N and south of 50°S at 200–10 hPa, while it increases north of 30°N, over 30°S–50°S, and below 500 hPa south of 30°S. In winter the geopotential height decreases north of 20°S and increases south of 20°S.

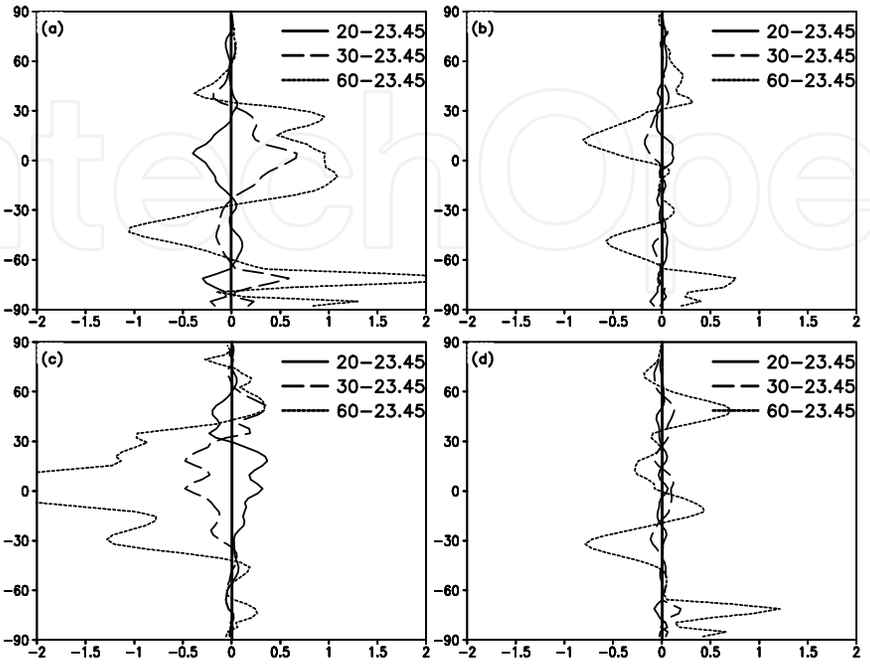

Figure 8. Same as Fig. 5 but for the seasonal mean. The solid line, dashed line, and short dotted line are for obliquities of 20°, 30°, and 60° minus 23.45°, respectively. a)–d) are the situations in winter, spring, summer, and autumn, respectively. Units: m s^{-1}.

The results for the temperature field with increased obliquity are as follows (figure not shown). In spring, there are cold anomalies (magnitude approximately 1 K) over 45°S–20°N, and warm anomalies south of 45°S and north of 20°N (the maximum warm anomaly can reach 2–3 K). In summer there are warm anomalies north of 10°N, and at 200–50 hPa over 30°S–10°N, while cold anomalies exist south of 10°N. In autumn the temperature decreases over 30°S–30°N and south of 30°S at 300–20 hPa, while it increases north of 30°N, above 30 hPa at 30°S–60°S, and south of 30°S below 300 hPa. In winter the temperature decreases north of 25°S and increases south of 25°S.

The zonal wind field responds to increased obliquity as follows (figure not shown). The extent of easterlies increases over the equator and easterly velocity strengthens, while the extent of westerlies decreases at middle latitudes. The jet stream strengthens at middle latitudes in the Southern Hemisphere while that in the Northern Hemisphere weakens. In spring, the wind strengthens in the stratosphere over the equator, while the easterlies weaken in the troposphere over the equator. The westerlies strengthen over 30°S–40°S below 200 hPa. In summer the extent and strength of easterlies increase in the stratosphere over the equator, but the easterlies weaken in the troposphere over the equator. The westerlies weaken in the Northern Hemisphere. The westerlies weaken at low latitudes (0°–30°S) in the Southern Hemisphere, strengthen at middle latitudes (30°S–60°S), and weaken at high latitudes (south of 60°S). In autumn the situation is similar to summer, with

increased extent and strength of easterlies in the stratosphere over the equator. Easterlies weaken in the troposphere over the equator, and in the Northern Hemisphere the westerlies weaken at middle–low latitudes (south of 60°N) and strengthen at high latitudes (north of 60°N). In winter the extent and velocity of easterlies increase in the stratosphere over the equator, while over the equator and globally, westerlies weaken.

Changes in the seasonal-mean vertical wind field are consistent with that of the three-cell circulation, and only the seasonal anomalies in the stratosphere resulting from increased obliquity are described here. In spring, ascending motion weakens over 0°–30°S, 80°S–90°S, and 70°N–80°N, while it strengthens over 0°–30°N. In summer, ascending motion weakens over 0°–30°S, south of 60°S, and north of 70°N, while it strengthens over 0°–50°N, and descending motion strengthens over 45°S–60°S. In autumn, ascending motion strengthens over 0°–30°S and weakens over 0°–30°N. In winter, descending motion strengthens over 0°–30°N and ascending motion strengthens over 0°–40°S. The descending motion over 40°S–60°S and ascending motion south of 70°S weaken.

3.4. Concluding remarks

The general circulation of the Earth's atmosphere has been simulated with different obliquities using the NCAR CAM2 model. The results indicate that the three-cell circulation weakens for large obliquity except in the Northern Hemisphere in winter, and the Hadley circulation in the Southern Hemisphere in spring and summer, which strengthen. The intensity of the annual mean three-cell circulation weakens for large obliquity. The extent of the Hadley circulation in the Southern Hemisphere increases, while that of the Hadley circulation in the Northern Hemisphere and the Ferrel circulation in the Southern Hemisphere decreases for large obliquity. The ascending branch of the Hadley circulation in the Southern Hemisphere strengthens significantly under the 60°-obliquity condition compared with the normal obliquity of the Earth. Both the annual mean extent and velocity of easterly winds in the stratosphere over the equator increase for large obliquity, whereas the extent of westerly winds decreases. The jet stream in the Northern Hemisphere weakens for large obliquity, while that in the Southern Hemisphere strengthens. In all four seasons, the easterlies in the troposphere and westerlies in the Northern Hemisphere weaken for large obliquity, as does the Northern Hemisphere mid-latitude jet stream. The differences in seasonal response for large obliquity are as follows. The mid-latitude jet stream in the Southern Hemisphere strengthens in spring, the westerly winds at middle and high latitudes change in opposite senses in summer and autumn in the Southern Hemisphere, and the global westerly winds are weaker in winter.

4. The influence of different orbit parameter on the monsoon

Generally the change of orbital parameter can modify the monsoon system by changing solar radiation. For example, Kutzbach and Otto-Bliesner (1982) analyzed the effect of orbital parameter change in Holocene on the African and Asian monsoon. The difference of radiation at two solstitial points are biggest the two solstitial points are closed related with

the monsoon, therefore the effects of different orbital parameters on the monsoon in summer and winter are analyzed. The results show that the monsoon in the Holocene was stronger than today and that precipitation in Africa and India were greater than today. In the 1980s, COHMAP, led by J. E. Kutzbach, T. Webb III, and H. E. Wright, was designed to determine and simulate paleoclimate using the land record. It revealed the key role of orbital factors in tropical monsoon climate change, and the bifurcation of the westerly jet stream over North America as a result of the ice cap in North America during the LGM period. Simulations show at the same time that the change of Earth's orbit in the early to middle Holocene led to a seasonal increase in the Northern Hemisphere and an enhanced monsoon (Kutzbach and Street-Perrott, 1985; Kutzbach and Guetter, 1986; Mitchell *et al*., 1988; Kutzbach, 1989; Kutzbach and Gallimore, 1989; Barron *et al*., 1993; Kutzbach *et al*., 1993; Rahmstorf, 1994; Barron *et al*., 1995; Rahmstorf, 1995; Kutzbach *et al*., 1996; Bush and Philander, 1997; Otto-Bliesner and Upchurch Jr, 1997; Ramstein *et al*., 1997; Weaver *et al*., 1998; Cane and Molnar, 2001; Knutti *et al*., 2004).

Can a change in rotation rate change the monsoon system? What is the effect of altering the obliquity on the monsoon system? In this section we seek to answer these questions using a unified dynamical index of the monsoon—the normalized seasonality and dynamical normalized seasonality (DNS), proposed by Li and Zeng (2000, 2002, 2003). The DNS is computed using the results in the previous two sections, to investigate the influence of the rotation rate and obliquity on the monsoon system. The normalized seasonality is given by

$$\delta = \frac{\left\| \overline{V_1} - \overline{V_7} \right\|}{\left\| \overline{V} \right\|} - 2,$$

where $\overline{V_1}$ and $\overline{V_7}$ are the mean January and July climatological wind vectors, respectively. $\overline{V}$ is the mean climatological wind vectors. The region of $\delta > 0$ represents the monsoon region. The DNS is given by

$$\delta^*_{m,n} = \frac{\left\| \overline{V_1} - \overline{V}_{m,n} \right\|}{\left\| \overline{\overline{V}} \right\|} - 2,$$

where $\overline{V}_{m,n}$ is the monthly wind vector for year n and month m.

4.1. The influence of different rotation rates on the global monsoon system

Figure 9 shows model output for the global normalized variability at 850 hPa. Compared with the control run (Fig. 9b), there is no obvious change in the extent of the tropical monsoon region and subtropical monsoon region, while the monsoon regions in the temperate and frigid zones change for both higher (Fig. 9a) and lower rotation rate (Fig. 9b).

The vertical distribution of the monsoon (Figs 10–14) shows no obvious change except for a slight movement of the edge of the monsoon region, but the strength of the monsoon clearly

changes. Because of the importance of the monsoon in the low level of the troposphere, Student's *t*-test was used to assess the statistical significance of the strength change of the monsoon at 850 hPa (Fig. 15). With faster rotation, the south and north African monsoons strengthen, while the tropical African monsoon weakens (Fig. 15c). In general, the African monsoon strengthens. Monsoons strengthen from the Arabian Sea to India, north of the Bay of Bengal, and from the southeast coast of China to the middle and lower reaches of the Yangtze River. At the same time, the monsoons in the Far East and North Pole region strengthen, while those in northeast Asia and from the south of the Bay of Bengal to the South China Sea and the East China Sea weaken. With slower rotation (Fig. 15a and b) the African monsoon, European monsoon, monsoon in the Far East, and monsoon in the North Pole region all weaken. Monsoons in the South China Sea and the East China Sea are still weakened. Monsoons in the Arabian Sea, Bay of Bengal, and north of Africa all strengthen. The African monsoon and the monsoons in the temperate zone and frigid zone weaken when the rotation rate slows, a reversal of the response to faster rotation. The Asian–Australian monsoon does not exhibit this reverse relationship. Globally, the monsoons do not change consistently with rotation rate.

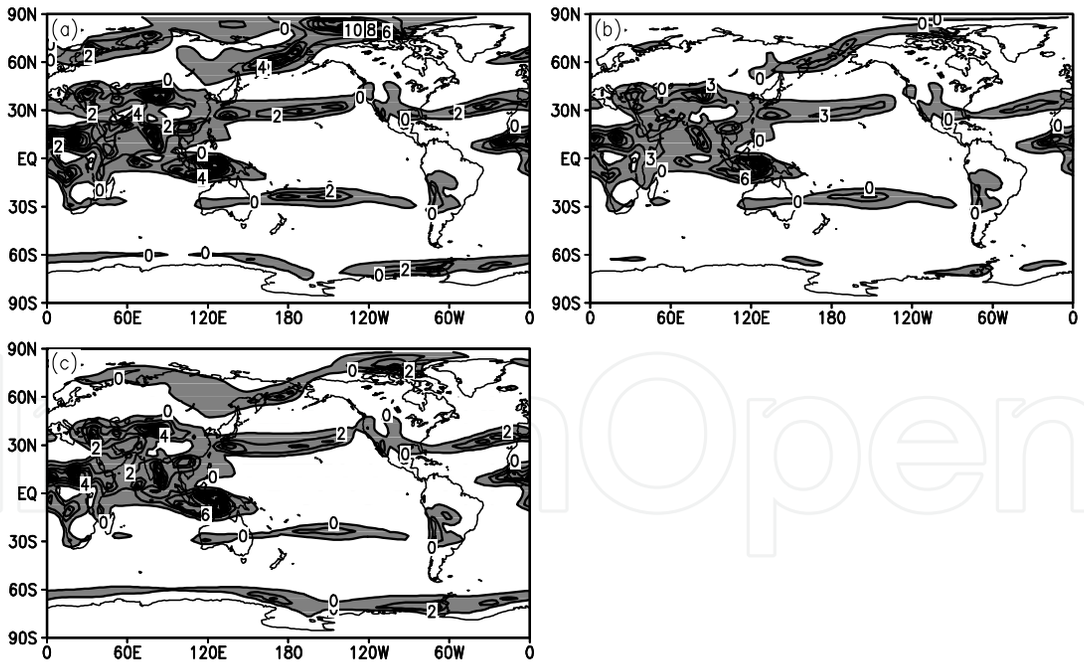

Figure 9. Global normalized variability at 850 hPa obtained from simulations. a) 23-hour day length; b) 24-hour day length; c) 25-hour day length. Shading indicates regions in which the normalized variability is greater than zero.

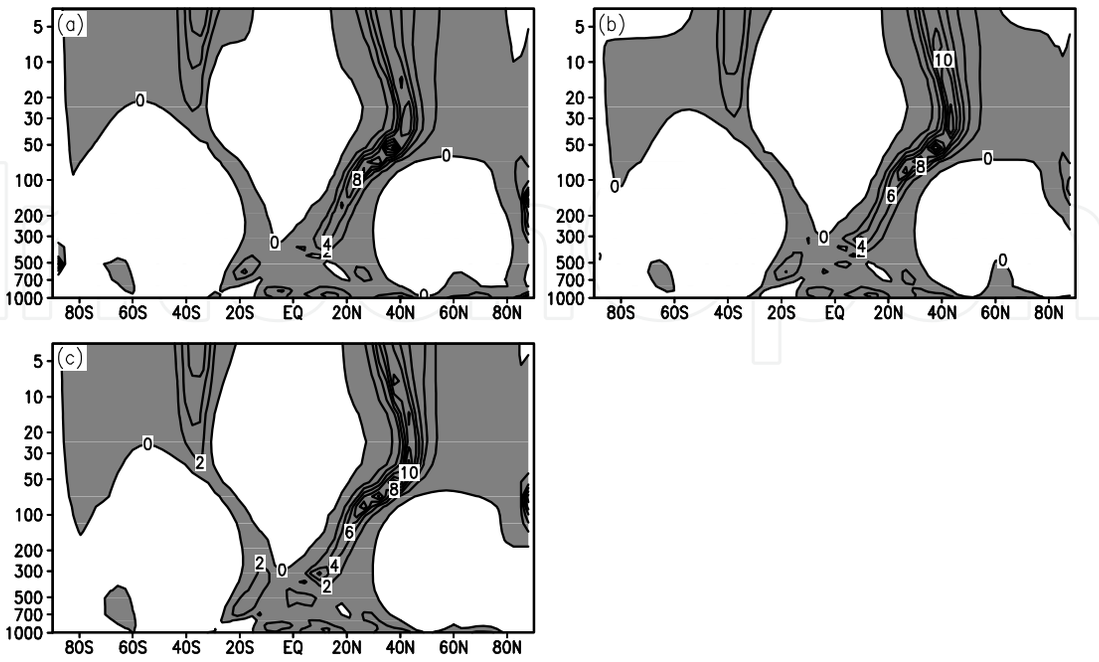

Figure 10. Latitude–pressure cross-section of zonal mean normalized variability. a) 23-hour day length; b) 24-hour day length; c) 25-hour day length. Shading indicates regions in which the normalized variability is greater than zero.

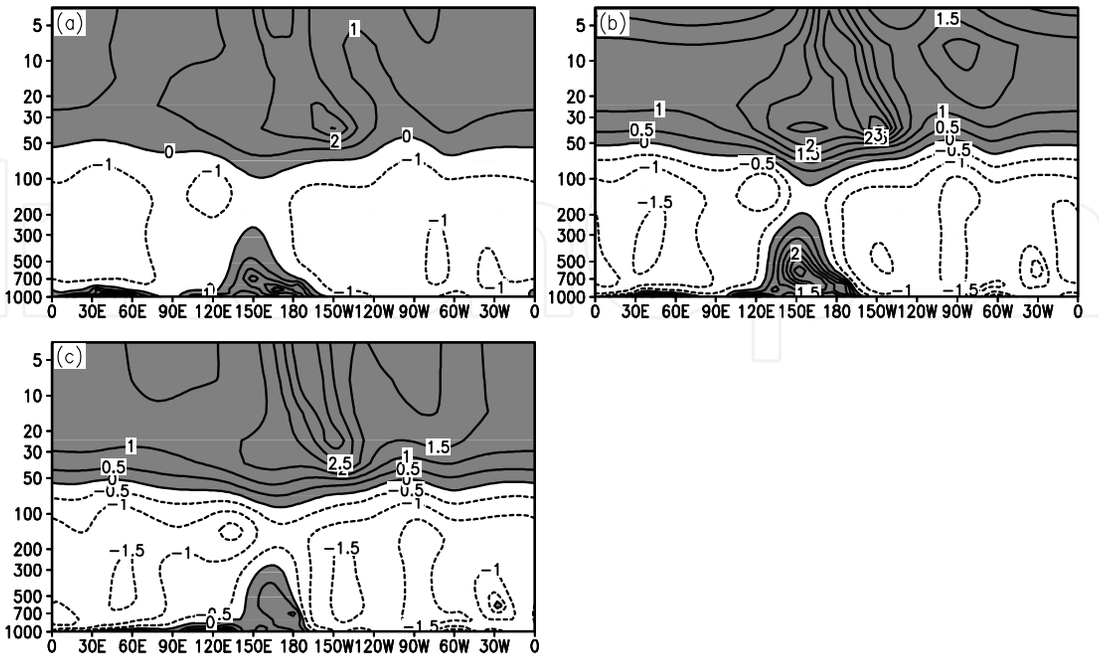

Figure 11. As Fig. 10, but for 50°N–70°N.

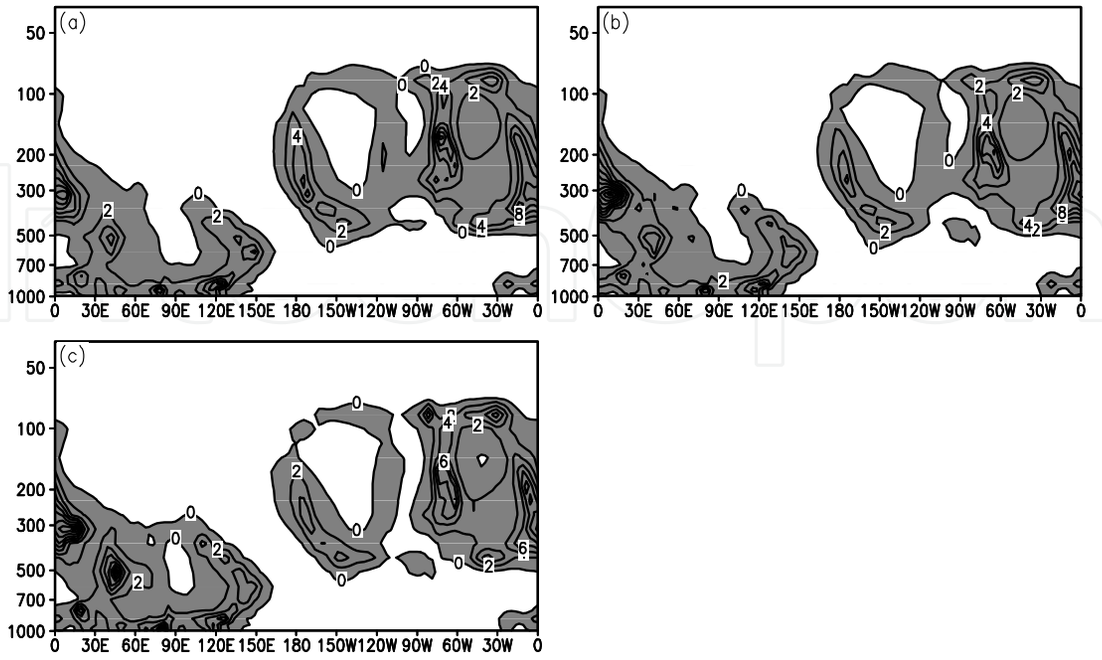

Figure 12. As Fig. 10, but for the tropics (10°S–10°N).

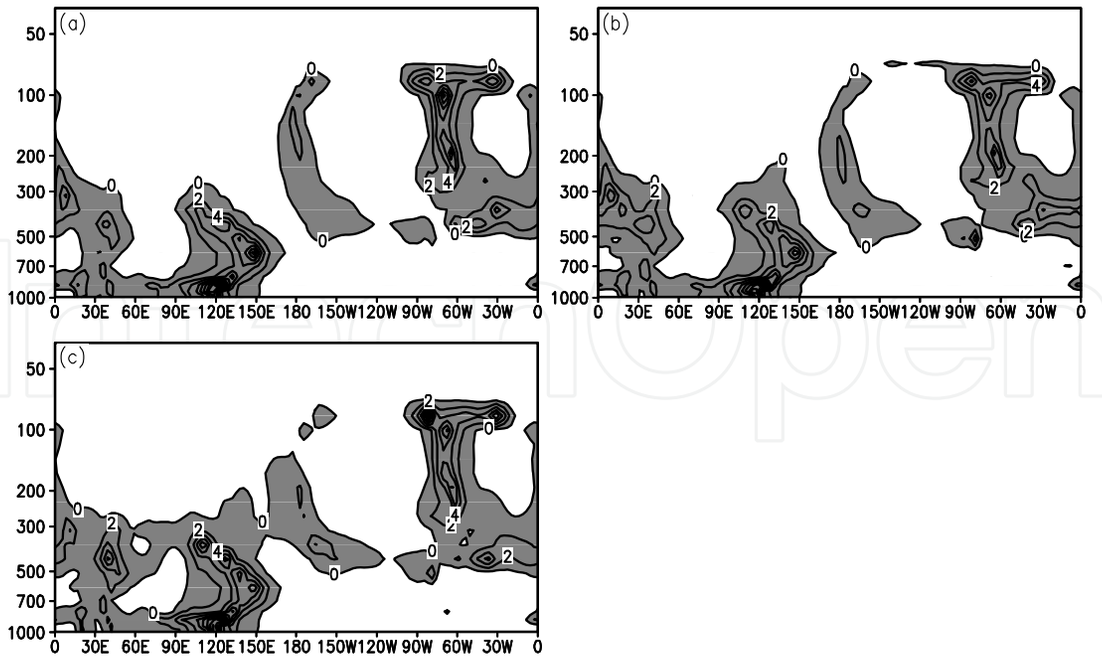

Figure 13. As for Fig.10, but for the tropical Southern Hemisphere (10°S–0°).

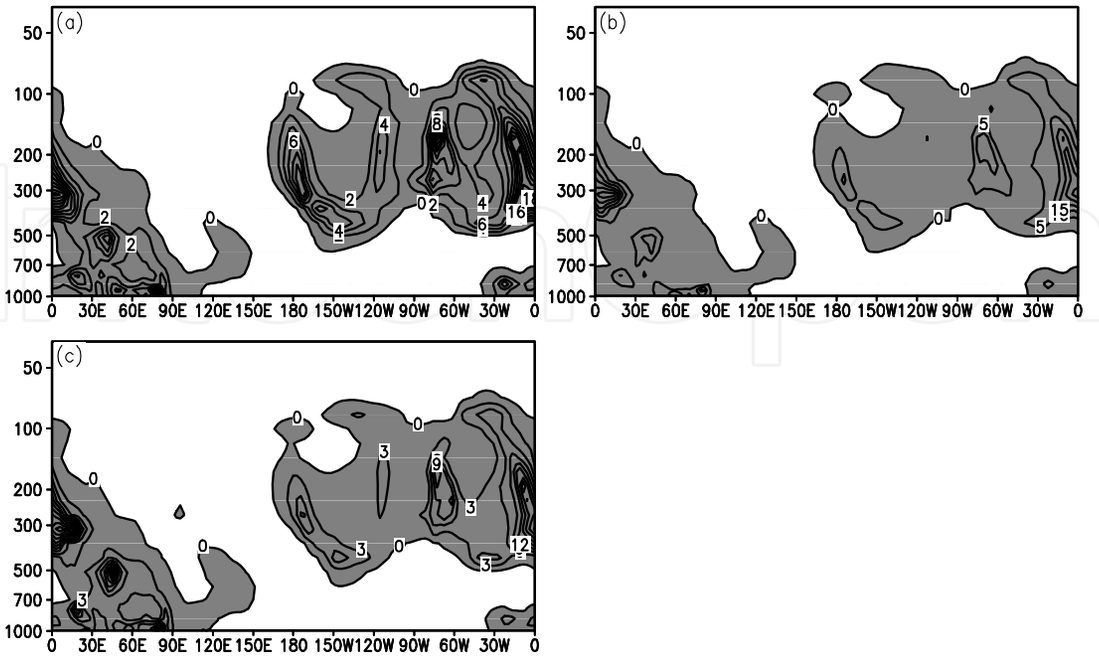

Figure 14. As for Fig. 10, but for the tropical Northern Hemisphere (0°–10°N).

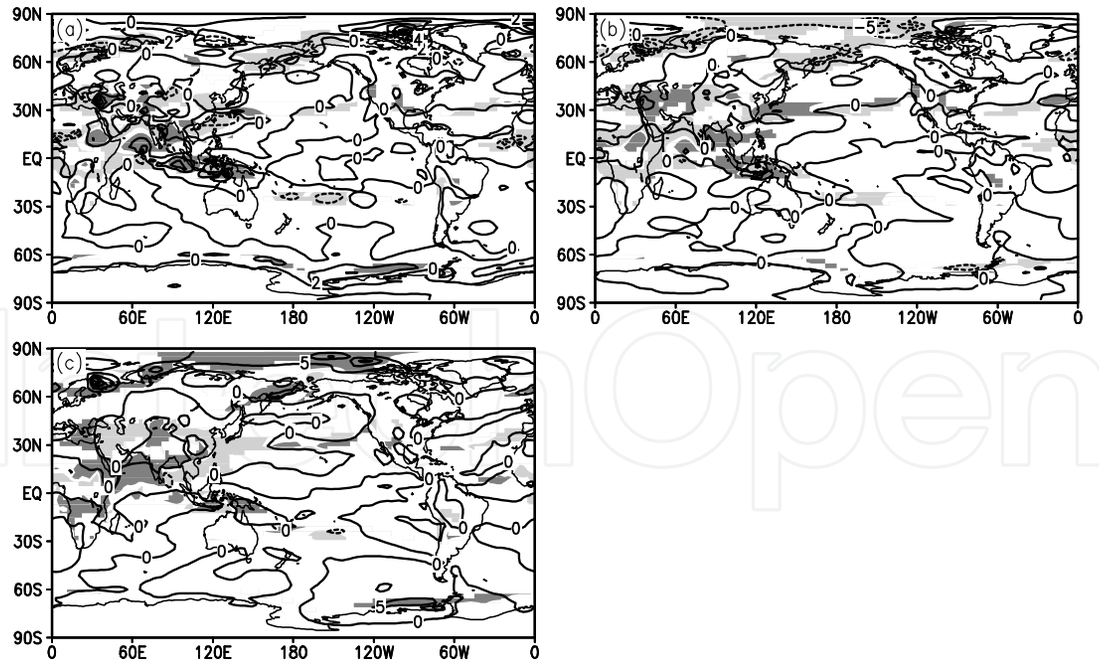

Figure 15. Normalized variability anomaly field, which is the sensitivity run minus the control run. (a) 25-hour day length minus 24-hour day length; (b) 25-hour day length minus 23-hour day length; (c) 23-hour day length minus 24-hour day length. Shading indicates statistically significant difference at the 95% level according to Student's *t*-test. Dark and light areas indicate positive and negative anomalies, respectively.

4.2. The influence of different obliquity on the global monsoon system

A change in obliquity will inevitably change the distribution of radiation; indeed, there is no seasonal variation with an obliquity of zero. Does the meridional wind reverse between January and July seasonally in the other sensitivity runs? Figure 16 shows the monthly-mean meridional winds over the domain 0°–10°N, 0°–120°E The meridional wind in January is opposite to that in June and July. Therefore, it is reasonable to use the DNS proposed by Li and Zeng (2000, 2002, 2003) and used in Section 4.1 to investigate the influence of obliquity on the monsoon system.

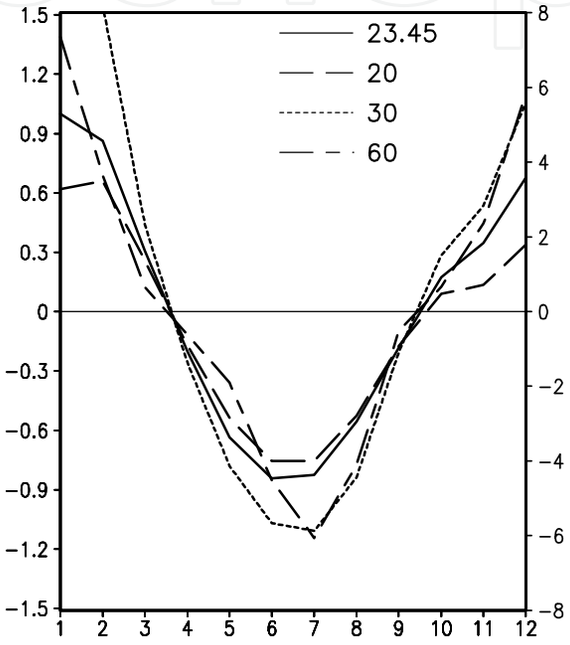

Figure 16. Monthly-averaged meridional winds over the domain 0°–10°N, 0°E–120°E. The horizontal axis shows the month of the year. The scale for meridional wind velocity for obliquities of 23.45°, 20° and 30° is on the left, and for obliquity of 60° on the right. Units are m s^{-1}.

Figure 17 shows the global normalized variability at 850 hPa obtained from the numerical simulations. Compared with the control run (Fig. 17d), the extent of the global monsoon region increases significantly with increased obliquity. The vertical distribution of the monsoon for different obliquities (Fig. 18) shows that the edge of the monsoon above 20 hPa in the stratosphere retreats to high latitudes with increased obliquity. At the same time, the monsoon in the stratosphere expands downward. It links up with the monsoon in the troposphere, which expands upward south of 60°S with increased obliquity. The monsoon in the stratosphere in the Northern Hemisphere also expands downward to the whole stratosphere. The monsoon in the Northern Hemisphere troposphere also expands.

In the temperate and frigid zones (50°N–70°N), the monsoon in the stratosphere extends down to the troposphere with increased obliquity, while that in the low troposphere extends slightly upward (Fig. 19). The tropical monsoon (10°S–10°N) (Fig. 20) expands at high levels with increased obliquity east of 180°E so that it covers the whole region from 500 hPa to 100

hPa east of 180°E. The part of the monsoon west of 180°E but east of 90°E expands westward and shrinks downward, while the part west of 90°E shrinks westward. The monsoon near the surface extends eastward to east of 150°E. For the tropical monsoon in the Southern Hemisphere (Fig. 21), the monsoon east of 90°W expands slightly horizontally. The monsoon over 180°E breaks up, and the western part shrinks horizontally and vertically. In particular, the tropical monsoon in the Northern Hemisphere (Fig. 22) expands with increased obliquity.

Because of the importance of the low-level monsoon, the significance of the *t*-test for the changes in monsoon strength at 850 hPa is also assessed here (Fig. 23). Figure 23 shows that the African, South American, North Pacific, and East Asian monsoons all strengthen with increased obliquity, and that the extent of the global monsoon increases. Furthermore, with decreased obliquity, the African, South American, North Pacific, and East Asian monsoons all weaken, and the extent of the global monsoon decreases. There is no obvious linear relationship with obliquity for monsoon strength in other regions. Therefore, the influence of obliquity on the monsoon in other region is perhaps indirect and non-linear.

In general, increased obliquity results in an increase in the extent of the global monsoon. This kind of change has a complex horizontal and vertical structure.

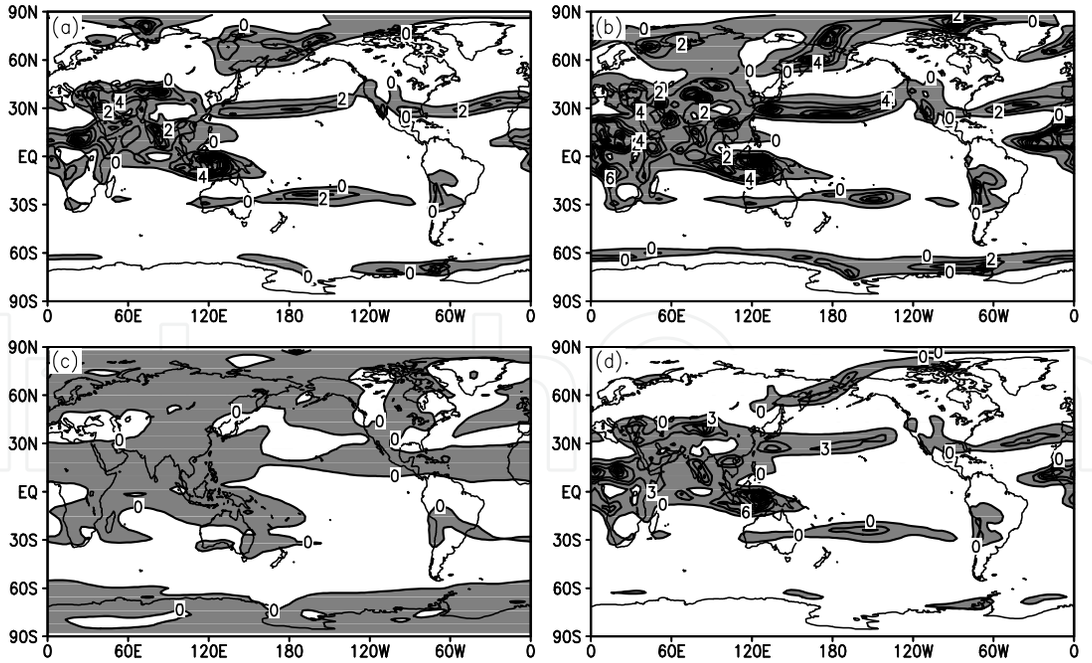

Figure 17. As for Fig. 9 but for different obliquity conditions. (a) 20° obliquity; (b) 30° obliquity; (c) 60° obliquity; (d) 23.45° obliquity.

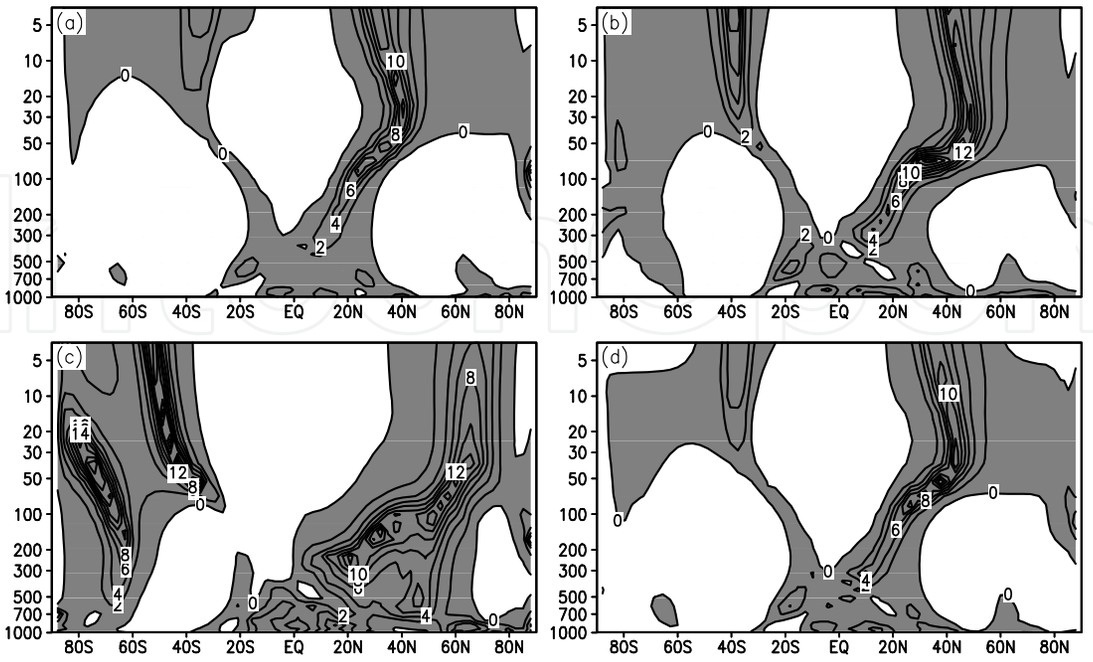

Figure 18. Zonal mean latitude–pressure cross-section. (a) 20° obliquity; (b) 30° obliquity; (c) 60° obliquity; (d) 23.45° obliquity.

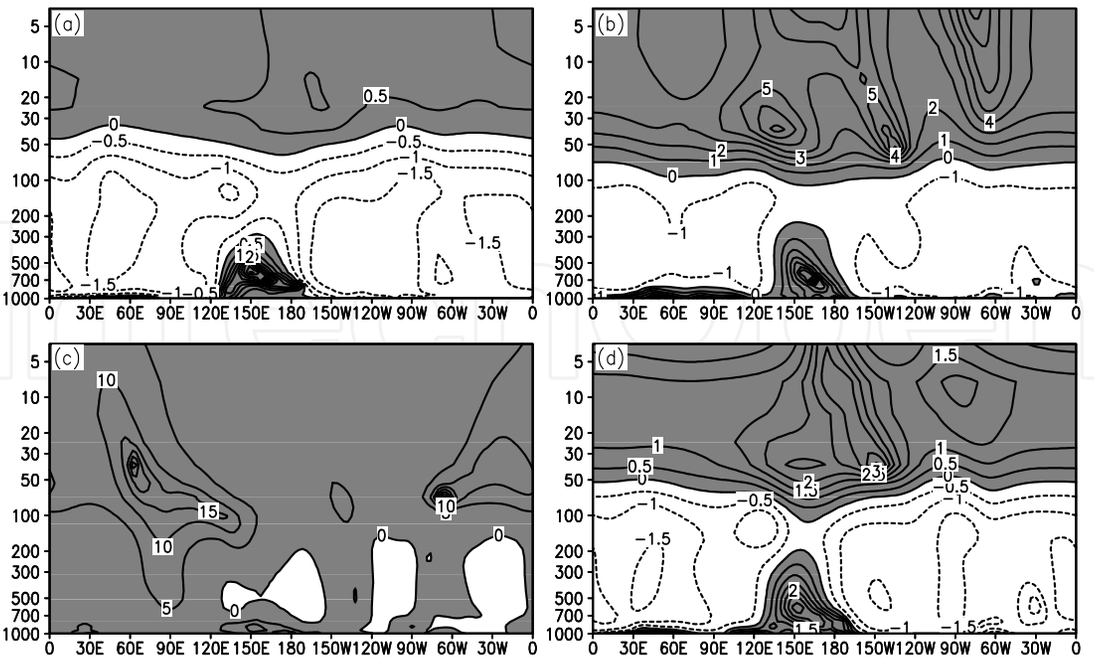

Figure 19. As for Fig. 18 but zonal cross-section for 50°N–70°N.

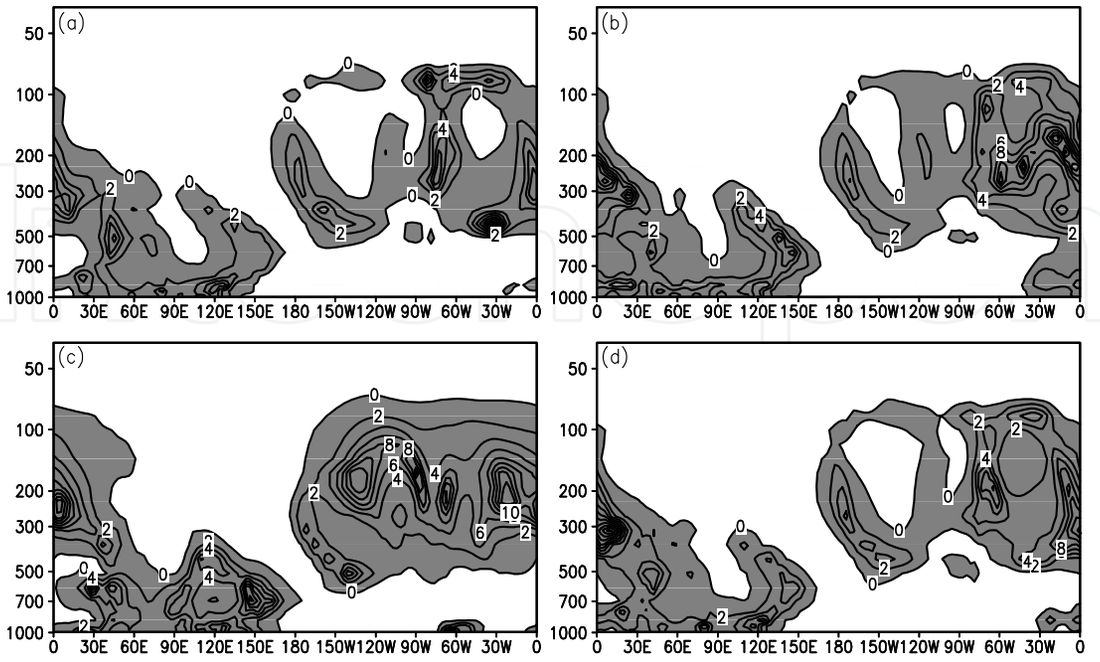

Figure 20. As for Fig. 18 but a tropical (10°S–10°N) latitude–pressure cross-section.

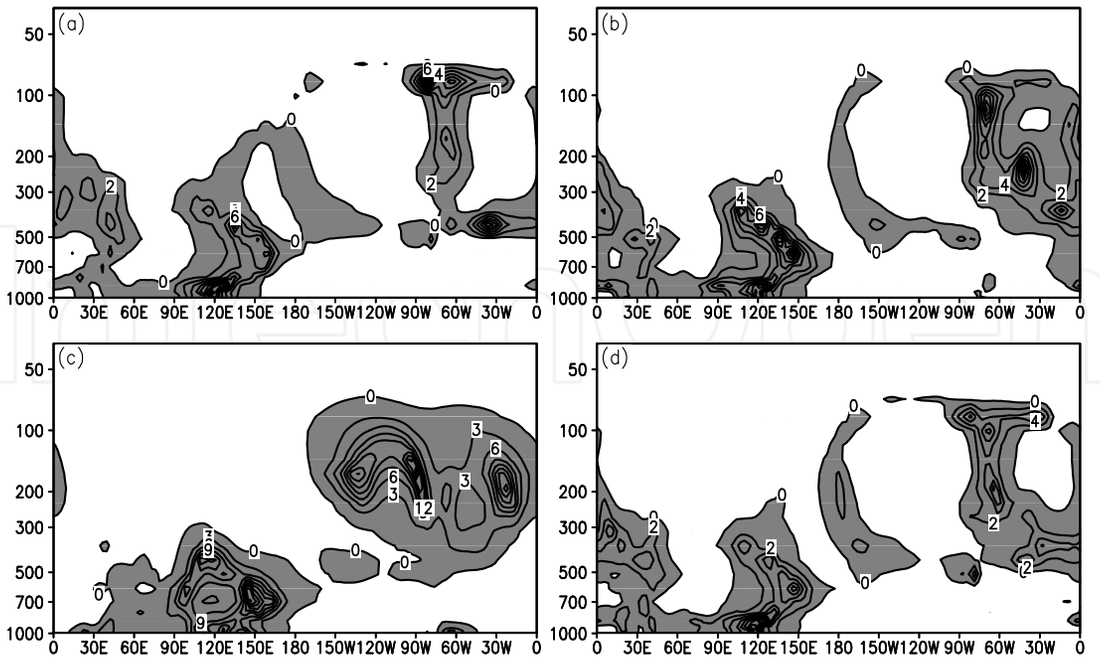

Figure 21. As for Fig. 18 but a Southern Hemisphere tropical latitude–pressure cross-section (10°S–0°).

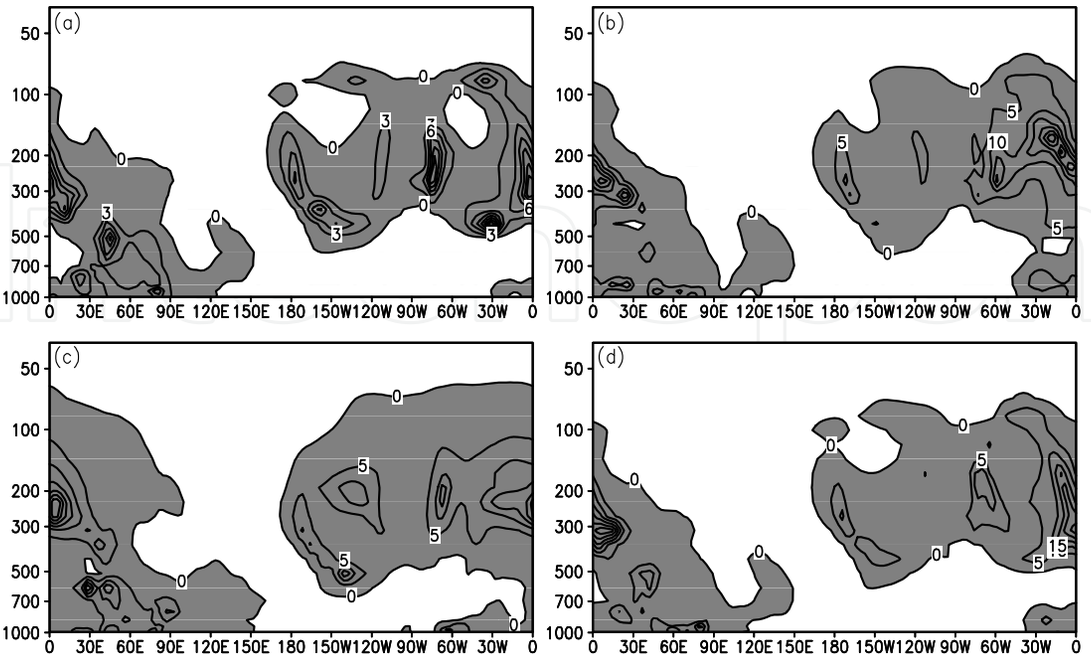

Figure 22. As for Fig. 18 but a Northern Hemisphere tropical latitude–pressure cross-section (0°–10°N).

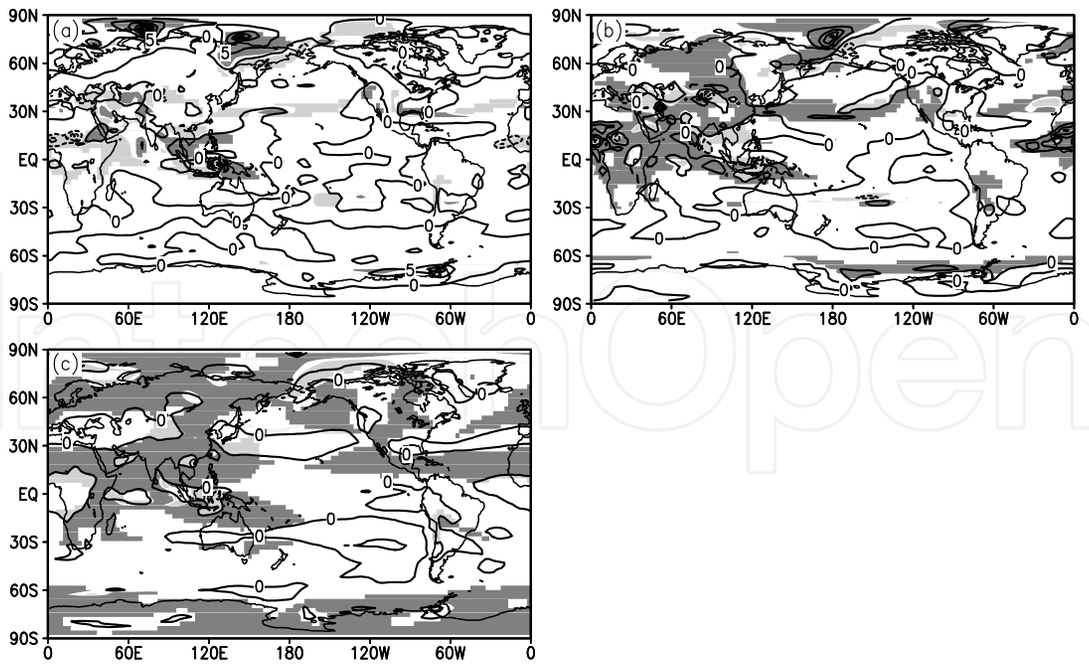

Figure 23. As for Fig. 15 but for different obliquity conditions. (a) 20° obliquity minus that of 23.45°; (b) 30° obliquity minus that of 23.45°; (c) 60° obliquity minus that of 23.45°. The shaded areas are significant at the 95% level according to Student's *t*-test. The dark and light areas indicate positive and negative anomalies, respectively.

4.3. Concluding remarks

There are three regions of linear response to the effect of rotation rate on the monsoon: Africa, the Middle East, and the temperate and frigid zones. For example, the African monsoon and the monsoon in the temperate and frigid zones weaken when the rotation rate slows. In general, with increased obliquity, the extent of the global monsoon is increased. This change also has a complex horizontal and vertical structure. At 850 hPa, the African, South American, North Pacific, and East Asian monsoons all strengthen with increased obliquity, and the extent of the global monsoon increases. At 850 hPa, with decreased obliquity, the African, South American, North Pacific, and East Asian monsoons all weaken, and the extent of the global monsoon decreases.

5. Results and discussion

The general circulation of the Earth's atmosphere has been simulated under different orbital parameters (rotation rate and obliquity). Retaining the same sea/land positions, we study the influence of orbital parameter on the three-cell circulation, potential height field, temperature field, wind field and monsoon on different timescales.

The results for the mean annual atmospheric circulation under different rotation rates are as follows:

1. The strength of the three-cell circulation is increased with the slower rotation compared with the higher rate, except for latitudes south of 80°S and 10°S–10°N, where the circulation weakens with slower rotation and strengthens with faster rotation, compared with the control run.
2. There are negative anomalies in the Northern Hemisphere annual mean temperature and positive anomalies in the Southern Hemisphere with the lower rotation rate, while the opposite is true for the faster case. The boundary between negative and positive anomalies is 15°S. Geopotential height changes in the same way as temperature for the different rotation rates.
3. Westerlies strengthen in the regions corresponding to 40°S–60°S and 40°N–60°N in the case of slow rotation, and weaken in other regions. The situation is reversed for faster rotation, but at slightly different latitudes. Westerlies strengthen in middle–high latitudes in both hemispheres for slow rotation. Compared with the control run, the easterlies strengthen and westerlies weaken over 15°S–30°S and below 700 hPa over 0°–30°N. Westerlies strengthen and easterlies weaken above 500 hPa over 30°S–70°S and 15°S–60°N. The situation reverses under faster rotation. Vertical velocities are enhanced in the troposphere and north of 30°S in the stratosphere for the lower rotation rate, while the vertical velocity weakens south of 30°S in the stratosphere. The situation under the higher rotation rate reverses, but the change is not completely symmetrical.

The results for the mean seasonal atmospheric circulation under different rotation rates are as follows:

1. The three-cell circulation strengthens for slow rotation and weakens for faster rotation, but the strengthening is not obvious in the Southern Hemisphere. Changes in autumn over the Southern Hemisphere, in the ascending branches of the Hadley cell over low latitudes (0°–25°S) and the Ferrel cell over high latitudes (60°S–90°S), which weaken for low rotation rate and strengthen for rapid rotation, are not consistent with those of other seasons. The largest changes of strength of the three-cell circulation occur in autumn, and for the Hadley cell, the second largest occur in winter. The changes in the mean annual three-cell circulation are driven by those in the seasonal mean three-cell circulation.
2. The change in autumn is the largest. The strength and extent of changes of geopotential height in autumn under different rotation rates are the largest. In spring, the changes with rotation rate in the geopotential height field, temperature field, and meridional wind field in the stratosphere and in the vertical velocity field are the opposite of the changes in summer and autumn (and annual mean). Westerlies in mid-latitudes strengthen in all four seasons with slower rotation. Changes in the zonal wind in both hemispheres are opposite in spring and autumn.

Results for the mean annual atmospheric circulation under different obliquity are as follows:

1. The intensity of the three-cell circulation weakens with increased obliquity. The ascending branch of the Hadley cell in the Southern Hemisphere strengthens with an obliquity of 60°. With increased obliquity, the Hadley cell in the Southern Hemisphere expands, and the Hadley cell in the Northern Hemisphere and the Ferrel cell in the Southern Hemisphere contract. Compared with the control run, the anomaly distributions are very similar between the sensitivity runs of 0° and 60° and those of 20° and 30°, while the anomaly magnitudes of 0° and 60° are larger than those of 20° and 30°. With increased obliquity, the three-cell circulation weakens linearly.
2. With decreased obliquity the geopotential height increases over 30°S–30°N, and decreases south of 30°S and north of 30°N. The change of geopotential height with obliquity change is asymmetrical in the Southern and Northern Hemispheres. Changes in the Northern Hemisphere are larger than in the Southern Hemisphere.
3. With decreased obliquity, the warm temperature anomalies mainly lie between 30°S and 30°N (reaching maximum values of 4 K and 1.2 K for 0° and 20° obliquity, respectively), while the cold anomalies lie south of 30°S and north of 30°N. The situation reverses for increased obliquity. With an obliquity of 0°, a zone of warm temperature anomaly at 10 hPa over the South Pole region extends northward and downward, reaching near the surface at 45°S. With an obliquity of 60°, the region of warm anomaly lies from 100 to 200 hPa over the equator.
4. With large obliquity, the extent of easterlies in the stratosphere increases and wind velocity strengthens. The extent of westerlies in both Southern and Northern Hemispheres decreases. The jet stream weakens in the Northern Hemisphere and strengthens in the Southern Hemisphere. Winds over other regions near the surface weaken, except over 10°S–10°N where the easterlies strengthen. The situation reverses with decreasing obliquity. In the mean annual meridional wind field, with increased

obliquity, southerlies weaken and northerlies strengthen south of 50°S in the stratosphere and north of 40°N. The northerlies weaken over 50°S–0° below 5 hPa in the stratosphere. The southerlies weaken over 0°–25°N. Northerlies strengthen above 5 hPa at 50°S–0° and southerlies strengthens above 5 hPa at 0°–25°N. Changes in the vertical wind in the troposphere are consistent with changes in the three-cell circulation and meridional wind field. With increased obliquity the vertical winds weaken. In the stratosphere, ascent strengthens over 45°S–65°S, 25°S–25°N, and 60°N–90°N, and weakens over 65°S–90°S. Descent strengthens over 25°S–45°S and 25°N–45°N.

The mean seasonal atmospheric circulation responds to changes in obliquity as follows:

1. In winter, with increased obliquity, the three-cell circulation in the Northern Hemisphere strengthens, and that in the Southern Hemisphere weakens. The three-cell circulation in the Northern Hemisphere weakens in spring, and the Hadley cell in the Southern Hemisphere strengthens. The other two cells weaken in the Southern Hemisphere in spring. In summer, the three-cell circulation weakens in the Northern Hemisphere, and the Hadley cell in the Southern Hemisphere strengthens. In this season, the changes of the other two cells are unclear. In autumn, the global three-cell circulation weakens. Changes in the three-cell circulation in the Northern Hemisphere in winter and the Hadley cell in the Southern Hemisphere in spring and summer are opposite to the corresponding changes in the annual mean. The changes in strength of the three-cell circulation in winter and summer are larger than in the other two seasons.
2. With increased obliquity, in spring the geopotential height decreases over 60°S–20°N, and increases south of 60°S and north of 20°N. In summer the geopotential height increases north of 30°N and over 40°S–30°N at 100–20 hPa, while it decreases below 100 hPa over 30°S–30°N, above 5 hPa both at 30°S–30°N and south of 30°S. In autumn, the geopotential height decreases over 30°S–30°N and south of 50°S at 200–10 hPa, while it increases north of 30°N, over 30°S–50°S, and below 500 hPa south of 30°S. In winter, geopotential height decreases north of 20°S and increases south of 20°S.
3. With increased obliquity, in spring there are cold temperature anomalies (magnitude approximately 1 K) over 45°S–20°N, and warm anomalies south of 45°S and north of 20°N (with maximum values of 2–3 K). In summer there are warm anomalies north of 10°N, and at 200–50 hPa over 30°S–10°N, while cold anomalies exist south of 10°N. In autumn the temperature decreases over 30°S–30°N and south of 30°S at 300–20 hPa. Temperatures increase north of 30°N, over 30 hPa at 30°S–60°S, and south of 30°S below 300 hPa. In winter the temperature decreases north of 25°S and the temperature increases south of 25°S.
4. With increased obliquity, in spring the zonal wind strengthens in the stratosphere over the equator. The easterlies weaken in the troposphere over the equator, while westerlies strengthen over 30°S–40°S below 200 hPa. In summer the extent of easterlies expands in the stratosphere over the equator, and the velocity of easterlies strengthens. The easterlies weaken in the troposphere over the equator, and the westerlies weaken in the Northern Hemisphere. Westerlies weaken at low latitudes (0°–30°S) in the Southern Hemisphere, strengthen at middle latitudes (30°S–60°S), and weaken at high latitude

(south of 60°S). In autumn the situation is similar to the summer, so that with increased obliquity, the extent and velocity of easterlies increase in the stratosphere over the equator. At the same time, easterlies weaken in the troposphere over the equator, and westerlies weaken at middle low latitudes (south of 60°N) and strengthen at high latitudes (north of 60°N) in the Northern Hemisphere. In winter, the extent and velocity of easterlies increase in the stratosphere over the equator, while the velocity over the equator and the global westerlies weaken.

5. Changes in the mean seasonal vertical wind field are consistent with those of the three-cell circulation. Responses in the stratosphere to increased obliquity are as follows. In spring, ascending motion weakens over 0°–30°S, 80°S–90°S, and 70°N–80°N, and strengthens over 0°–30°N. In summer, ascending motion weakens over 0°–30°S, south of 60°S, and north of 70°N, and strengthens over 0°–50°N while the descending motion strengthens over 45°S–60°S. In autumn, ascending motion strengthens over 0°–30°S and weakens over 0°–30°N. In winter, descending motion strengthens over 0°–30°N and ascending motion strengthens over 0°–40°S. The descending motion over 40°S–60°S and ascending motion south of 70°S are weakened.

Results for the monsoon system are as follows:

1. There is no obvious change in the extent of the tropical and subtropical monsoon regions under different rotation rates, while the monsoon region in the temperate and frigid zones clearly changes. The vertical distribution of monsoon does not appear to change except for a slight movement of the edge of the monsoon region. The monsoon strength clearly changes with different rotation rates. Both the southern and northern parts of the African monsoon strengthen with rapid rotation, while the tropical African monsoon weakens. Monsoons strengthen from the Arabian Sea to India, north of the Bay of Bengal, and from the southeast coast of China to the middle and lower reaches of the Yangtze River. At the same time, the monsoons in the Far East and North Polar Region strengthen, while the monsoons in northeast Asia and from south of the Bay of Bengal to the South China Sea and the East China Sea weaken. With slow rotation the African and European monsoons, as well as the monsoon in the Far East and in the North Polar Region all weaken. Monsoons in the South and East China Sea still weaken. Monsoons in the Arabian Sea, Bay of Bengal, and north of Africa are all strengthened. The African monsoon and the monsoon in the temperate and frigid zones weaken when the rotation rate reduces. The situation is reversed with faster rotation. The Asian–Australian monsoon does not exhibit this reverse relationship. Globally, the monsoons do not change consistently with rotation rate.
2. With increased obliquity, the extent of the global monsoon increases. This change has complex horizontal and vertical structure. With increased obliquity, at 850 hPa, the African, South American, North Pacific, and East Asian monsoons all strengthen, and the global monsoon increases in extent. With decreased obliquity, at 850 hPa, the African, South American, North Pacific, and East Asian monsoons all weaken, and the extent of the global monsoon decreases.

The present results indicate that the influence of obliquity or rotation rate change on general circulation can be evaluated under the assumptions that the land–sea distribution does not change and that the terrain height remains the same. The results can help us to discover which factors, obliquity or rotation rate, are responsible for the circulation anomalies in simulations of paleoclimate. At the same time, analyzing the influence of individual orbital parameters on geophysical fields for each of the four seasons helps us to better understand the laws governing components of climate change in geological periods. Investigation of the influence of variation in individual orbital parameters on the monsoon can deepen our knowledge of the monsoon.

6. Conclusion

Our results indicate that the three-cell circulation strengthens when the Earth's rotation rate slows. Furthermore, there are cool anomalies in the annual mean temperature field in the Northern Hemisphere and warm anomalies in the Southern Hemisphere for the lower rotation rate. The boundary between regions of cool and warm anomalies is located at 15°S. The sign of the annual mean zonal wind field anomalies changes when the rotation rate is changed. The positive and negative anomalies reverse between lower and higher rotation rates. The changes in the geopotential height field, temperature field, and meridional wind field in the stratosphere and in the vertical velocity field in spring are opposite to those in summer and autumn (and in the annual mean) under different rotation rates. Mid-latitude westerlies strengthen in all four seasons with a low rotation rate. Changes in the zonal wind in the two hemispheres reverse in spring and autumn. Quantitative changes show significant seasonal variation, with the largest changes in autumn. There are three regions of linear monsoon response to changing rotation rate: Africa, the Middle East, and the temperate and frigid zones.

Our results suggest that the three-cell circulation weakens for large obliquity, except for the three-cell circulation in the Northern Hemisphere in winter, and the Hadley circulation in the Southern Hemisphere in spring and summer, which strengthen with increased obliquity. The annual mean three-cell circulation weakens for large obliquity. The annual mean Hadley circulation in the Southern Hemisphere expands for large obliquity while the Hadley circulation in Northern Hemisphere and the Ferrel circulation in Southern Hemisphere shrink for large obliquity. The ascending branch of the Hadley circulation in the Southern Hemisphere strengthens significantly when the obliquity is increased from its normal value to 60°. The annual mean extent and velocity of easterly winds in the stratosphere over the equator increase for large obliquity, but the extent of the westerly winds decreases. The jet stream weakens in the Northern Hemisphere and strengthens in the Southern Hemisphere. In all four seasons, the easterlies in the troposphere and westerlies in the Northern Hemisphere weaken, and the mid-latitude jet stream in the Northern Hemisphere weakens for large obliquity. The strength of the mid-latitude jet stream in the Southern Hemisphere strengthens in spring, the westerly wind at middle and high latitudes changes in opposite senses in summer and autumn in the Southern Hemisphere, while the westerly wind weakens globally in winter.

The global monsoon expands with increased obliquity, and the African, South American, North Pacific and East Asian monsoons strengthen.

From the above, we can conclude that rotation rate and obliquity can have a significant effect on the general circulation of the Earth's atmosphere and on the monsoon system. This may partly explain changes in the atmosphere that have occurred as the Earth has evolved. By this means, we can determine where the responses to changing orbital parameters are linear or nonlinear. Of course these experiments are not enough by themselves. Additional experiments are required in which we change the land–sea distribution, the topography, and make simultaneous changes to more than one orbital parameter, to further determine the linearity of the response. These experiments will require extensive numerical simulations. In addition, the thermal contrast between land and sea can have a significant effect on the monsoon and atmospheric circulation. Further simulations with air–sea coupled models will deepen our knowledge of the monsoon and atmospheric circulation. All of these studies can help us to design further simulations to investigate and understand the Earth's changing climate.

Author details

Xinhua Liu
National Meteorological Center (NMC), Beijing, China
Key Laboratory for Semi-Arid Climate Change of the Ministry of Education, Lanzhou University, Lanzhou, China

Acknowledgement

The author of this chapter is grateful to the editor and the reviewer for their helpful comments and suggestions that greatly improved the manuscript. This study is jointly supported by the National Science Foundation of China (41105026) and the Foundation of Key Laboratory for Semi-Arid Climate Change of the Ministry of Education in Lanzhou University (the Fundamental Research Funds for the Central Universities Programs for Science and Technology Development of China, 223-860011). I also thank Professor Jianping Li and Athena Coustenis for their instructions and guidance.

7. References

Barron, E. J., P. J., Fawcett, D., Pollard, et al., 1993: Model simulations of Cretaceous climates: the role of geography and carbon dioxide. Philos. Trans. R. Soc. London B, 341, 307-316.

Barron, E. J., P. J., Fawcett, W. H., Peterson, et al., 1995: A 'simulation' of mid-Cretaceous climate. Paleoceanography, 10, 953-962.

Berger A., J. Imbrie, J. Hays, et al., 1984: Milankovitch and Climate. D Reidel Publishing Company, Dordrecht, Boston, Lancaster.

Bush, A. B. G., S. G. H., Philander, 1997: The late Cretaceous: Simulation with a coupled atmosphere-ocean general circulation model. Paleoceanography, 12, 495-516.

Cane, M. A., P., Molnar, 2001: Closing of the Indonesian seaway as a precursor to east African aridification around 3-4 million years ago. Nature, 411, 157-162.

Clemens, S. C., W., Prell, D., Murray, et al., 1991: Forcing mechanisms of the Indian Ocean Monsoon. Nature, 353, 720-725.

Collins, W.D., J.J., Hack, B.A., Boville, P.J., Rasch, D.L., Williamson, J.T., Kiehl, B., Briegled, J.R., Mccaa, C., Bitz, S-J., Lin, R.B., Rood, M.H., Zhang, Y.J., Dai, 2003: Description of the NCAR Community Atmosphere Model (CAM2). Boulder, Colorado, http:// www.ccsm.ucar.edu/models/atm-cam/docs/cam2.0/description/index.html.

Del Genio, A. D., W., Zhou, 1996: Simulations of superrotation on slowly rotating planets: sensitivity to rotation and initial condition. Icarus, Vol 120, pp.332-343.

Gates, W. L., 1976: Modeling the ice age climate. Science, 191, 1138-1144.

Hall, A., A., Clement, D. W. J., Thompson, A., Broccoli, C., Jackson, 2005: The Importance of Atmospheric Dynamics in the Northern Hemisphere Wintertime Climate Response to Changes in the Earth's orbit. J. Clim., 18, 1315-1325.

Hourdin, F., O., Talagrand, R., Sadourny, R., Courtin, D., Gautier, C.P., McKay, 1995: Numerical simulation of the general circulation of the Titan. Icarus, Vol 117, pp.358-374.

Hunt, B.G., 1979: The influence of the earth's rotation rate on the general circulation of the atmosphere. J. Atmos. Sci., 36, 1392-1407.

Jenkins, G. S., 1993: A general circulation model study of the effects of faster rotation, enhanced CO2 concentrations and reduced solar forcing: Implications for the Faint-Young Sun Paradox. J. Geophys. Res., 98, 20803-20811.

Jenkins, G. S., 1996: A sensitivity study of changes in Earth's rotation with an atmospheric general circulation model. Global Planet. Change, 11, 141-154.

Jenkins, G. S., H. G., Marshall, W. R., Kuhn, 1993: Precambrian climate: The effects of land area and Earth's rotation rate. J. Geophys. Res., 98, 8785-8791.

Jian, Z., B., Huang, W., Kuhnt, et al., 2001: Late quatemary upwelling intensity and East Asian monsoon forcing in the South China Sea. Quatemary Research, 55, 363-370.

Joussaume, S., K. E., Taylor, 1995: Status of the paleoclimate modeling intercomparison project (PMIP). Proceedings of the first international AMIP scientific conference (WCRP Report, 1995), 425-430.

Kutzbach, J. E., B. L., Otto-Bliesner, 1982: The sensitivity of the African-Asian monsoonal climate to orbital parameter changes for 9000 years B.P. in a low-resolution general circulation model. J. Atmos. Sci., 39, 1177-1188.

Knutti, R., J., Fluckiger, T. F., Stocker, et al., 2004: Strong hemispheric coupling of glacial climate through fresh water discharge and ocean circulation. Nature, 430, 851-856.

Kutzbach, J. E., F. A., Street-perrott, 1985: Milankovitch forcing of fluctuations in the level of tropical lakes from 18~0 kyr BP. Nature, 317, 130-134.

Kutzbach, J. E., G., Bonan, J., Foley, et al., 1996: Vegetation and soil feedbacks on the response of the African monsoon to orbital forcing in the Early to Middle Holocene. Nature, 384, 623-626.

Kutzbach, J. E., P. J., Guetter, 1986: The influence of Changing orbital parameters and surface boundary conditions on climate simulations for the past 18000 years. J. Atmos. Sci., 43, 1726-1759.

Kutzbach, J. E., P. J., Guetter, W. F., Ruddiman, et al., 1989: The sensitivity of climate to late Cenozoic uplift in south-east Asia and the American southwest: Numerical experiments. J. Geophys. Res., 94, 18393-18407.

Kutzbach, J. E., R. G., Gallimore, 1989: Pangean climates: Megamonsoons of the megacontinent. J. Geophys. Res., 94 (D3), 3341-3357.

Kutzbach, J. E., W. L., Prell, W. F., 1993: Ruddiman, Sensitivity of Eurasian climate to surface uplift of the Tibetan plateau. The Journal of Geology, 101, 177-190.

Kutzbach, J. E., Z., Liu, 1997: Response of the African monsoon to orbital forcing and ocean feedbacks in the middle Holocene. Science, 278, 440-443.

Li, J., and Q. Zeng, 2003: A new monsoon index and the geographical distribution of the global monsoons. *Adv. Atmos. Sci.,* 20, 299-302.

Li, J., and Q. Zeng, 2002: A unified monsoon index. Geophys. Res. Lett., 29(8), 1274, doi:10.1029/2001GL013874.

Li, J., and Q. Zeng, 2000: Significance of the normalized seasonality of wind field and its rationality for characterizing the monsoon. *Sci. China (Ser. D),* 43(6), 646-653.

Liu, Xinhua, Jianping Li, Qingliang Zhou and Yi Yang, 2010: Numerical simulation of the influence of changing rotation rate on the general circulation of the Earth's atmosphere. Information Science and Engineering (ICISE), 2010 2nd International Conference on, 5203-5206, 10.1109/ICISE.2010.5691888.

Liu. Xinhua, 2011: Numerical simulation of atmospheric general circulation under different obliquity of Earth. 2011 International Conference on Remote Sensing, Environment and Transportation Engineering, RSETE 2011 - Proceedings, p 5115-5118.

Mitchell, J. F. B., N. S., Grahame, K. H., Needham, 1988: Climate simulation for 9 000 years before present: Seasonal variations and the effects of Laurentide ice sheet. J. Geophys. Res., 93, 8283-8303.

Oort, A. H., J. J., Yienger, 1996: Observed interannual variability in the Hadley circulation and its connection to ENSO. J. Climate., Vol 9, pp.2751-2767.

Otto-bliesner, B. L., G. R., Upchurch Jr, 1997: Vegetation induced warming of high-latitude regions during the Late Cretaceous period. Nature, 385, 804-807.

Prell, W. L., J. E., Kutzbach, 1997: The impact of Tibet-Himalayan elevation on the sensitivity of the monsoon climate system to changes in solar radiation. Ruddiman, W. F., Tectonic uplift and climate change. New York: Plenum Press, 171-201.

Qian, W. H., 1995: The observational study and numerical experiment on the effect of the variation of the earth's rotation on the global sea surface temperature anomaly. Chinese J. Atmos. Sci., Vol. 19, pp.654-662.

Quan, X. W., H. F., Diaz, M. P., Hoerling, 2004: Change in the tropical Hadley cell since 1950, in the Hadley Circulation: Past, Present, and Future, edited by H. F. Diaz and R. S. Bradley, Cambridge Univ. Press, New York.

Rahmstorf, S., 1994: Rapid climate transitions in a coupled ocean-atmosphere model. Nature, 372, 82-85.

Rahmstorf, S., 1995: Bifurcations of the Atlantic thermohaline circulation in response to changes in the hydrological cycle. Nature, 145-149.

Ramstein, G., F., Fluteau, J., Besse, et al., 1997: Effect of orogeny, plate motion and land-sea distribution on Eurasian climate change over the past 30 million years. Nature, 386, 788-795.

Tuenter, E., S. L., Weber, F. J., Hilgen, L. J., Lourens, 2003: The response of the African summer monsoon to remote and local forcing due to precession and obliquity. Global and Planetary Change, 36, 219-235.

Weaver, A. J., M., Eby, A. F., Fanning, et al., 1998: Simulated influence of carbon dioxide, orbital forcing, and ice sheets on the climate of the last glacial maximum. Nature, 394, 847-853.

Williams, J. R. G., R. G., Barry, W. M., Washington, 1974: Simulation of the atmospheric circulation using the NCAR global circulation model with ice age boundary conditions. J. Appl. Meteorol., 13, 305-317.

Williams, G. E., Megacycles, 1981: Long-Term Episodicity in Earth and Planetary History. Hutchinson Ross Publishing Company, Stroudsburg, Pennsylvania.

Zheng, D. W., G., Chen, 1994: Relation between equatorial oceanic activities and LOD changes. Science in China (A), 37, 341-347.